

Theoretical and experimental study of the vibration of axisymmetric viscous liquid bridges

J. M. Perales and J. Meseguer

Lamf-µg, Laboratorio de Aerodinámica, E.T.S.I. Aeronáuticos, Universidad Politécnica, 28040 Madrid, Spain

(Received 9 May 1991; accepted 10 February 1992)

In this paper the dynamics of axisymmetric liquid columns held by capillary forces between two circular, concentric, solid disks is considered. The problem has been solved by using a one-dimensional model known in the literature as the Cosserat model, which includes viscosity effects, where the axial velocity is considered constant in each section of the liquid bridge. The dynamic response of the bridge to an excitation consisting of a small-amplitude vibration of the supporting disks has been solved by linearizing the Cosserat model. It has been assumed that such excitation is harmonic so that the analysis has been performed in the frequency domain. The particular case of a cylindrical liquid bridge has been analytically studied and the transfer function has been calculated in the cases of oscillation of both disks (either in phase or in counterphase) or only of one of them. The resolution of the general formulation for a noncylindrical liquid bridge has been numerically made by using an implicit finite difference method. In this case, the influence of the volume of the liquid column and of the residual gravity level on the first resonance has been studied, and the results compared, for the inviscid case, with other potential models, both one and three dimensional. To demonstrate the usefulness of this theoretical model in predicting the vibrational behavior of axisymmetric viscous liquid bridges, some experiments have been performed by using the neutral buoyancy technique (also known as the Plateau technique) to simulate reduced gravity conditions, with good agreement between the results of the model and experiments.

I. INTRODUCTION

A liquid bridge is an idealization of the fluid configuration appearing in the crystal growth technique, known as floating zone melting (Wilcox¹). The liquid bridge configuration, as sketched in Fig. 1, consists of a mass of liquid held by surface tension forces between two parallel, coaxial, solid disks. Such fluid configuration can be identified by the following dimensionless parameters: the slenderness, $\Lambda = L/2R_0$, where L is the distance between the disks and $R_0 = (R_1 + R_2)/2$ is the mean radius, R_1 and R_2 being the radii of the supporting disks, the ratio of the radius of the smaller disk to the radius of the larger one, $K = R_1/R_2$, the dimensionless volume of liquid, $V = V/R_0^3$, V being the physical volume, the Bond number, $B = \rho g R_0^2/\sigma$, and the capillary number (equal to the square root of the Ohnesorge number, Oh), $C = \nu(\rho/\sigma R_0)^{1/2} = Oh^{1/2}$, where ρ is the liquid density, g is the axial acceleration, σ is the surface tension, and ν is the kinematic viscosity.

The availability of fluid mechanics experiments in space has given rise to the study of the behavior of liquids under microgravity conditions (Myshkis *et al.*²), the liquid bridge being one of the fluid configurations that is receiving increasing attention in those experiments. Many mechanical aspects of the liquid bridge problem have been extensively studied, both from a theoretical and an experimental point of view. The stability of liquid bridges between equal disks has been studied by Haynes;³ Erle, Gillette, and Dyson;⁴ Gillette and Dyson;⁵ Coriell and Cordes;⁶ Martínez;⁷ Boucher and Evans;⁸ Slobozhanin;⁹ Russo and Steen;¹⁰ Perales;¹¹ and

Boucher and Jones,¹² among others. Some works deal with the effect of either unequal disks (Coriell, Hardy, and Cordes;¹³ Da Riva and Martínez;¹⁴ Meseguer;^{15,16} Martínez and Perales;¹⁷ and Meseguer, Sanz, and Perales¹⁸), nonanchored interfaces (Martínez^{7,19}) or nonplanar supporting disks (Martínez²⁰). The effect of the rotation on the stability has been studied by Brown and Scriven;²¹ Da Riva;²² Ungar and Brown;²³ Vega and Perales;²⁴ and Perales, Sanz, and Rivas;²⁵ whereas the effect of the gravity on short bridges has

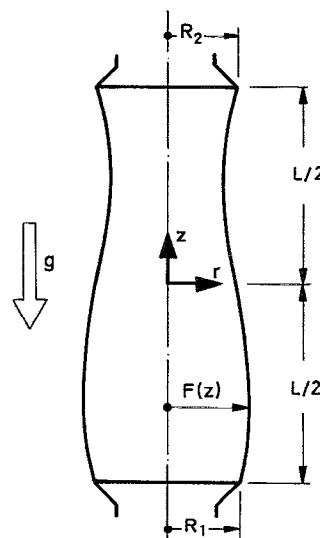


FIG. 1. Geometry and coordinate system for the liquid bridge problem.

been studied by Heywang;²⁶ Martínez and Perales;²⁷ and Perales, Meseguer, and Martínez.²⁸

The dynamics of the liquid bridge has been studied by using three-dimensional linearized models by Sanz;²⁹ Bauer;^{30,31} Gañán;³² and Sanz and López-Diez;³³ among others. Some attempts have been made to solve the problem of the dynamics of the liquid bridge when the supporting disks rotate (Da Riva and Meseguer;³⁴ Da Riva and Manzano;³⁵ Harriot and Brown;^{36,37} etc.). In order to simplify the problem formulation a one-dimensional slice model has been used by Meseguer;³⁸⁻⁴¹ Meseguer, Sanz, and Rivas;⁴² Meseguer and Sanz;^{43,44} Sanz;²⁹ Meseguer, Sanz, and Perales;¹⁸ Zhang and Alexander;⁴⁵ etc. A more elaborated one-dimensional model, derived from the Cosserat formulation, has been used by Meseguer;³⁸ Rivas and Meseguer;⁴⁶ Meseguer *et al.*;¹⁸ and Meseguer and Perales,⁴⁷ leading to predictions in good agreement with experimental results.

The experimental determination of the minimum volume stability limit has been made, for different configurations, by Mason;⁴⁸ Sanz and Martínez;⁴⁹ Meseguer *et al.*;⁵⁰ Meseguer and Sanz;⁴³ and Perales *et al.*,²⁸ whereas the maximum volume stability limit has been measured by Russo and Steen.¹⁰ The breaking process dynamics has been studied by Meseguer and Sanz;⁴³ and Meseguer, Sanz, and López;⁵¹ and the liquid bridge formation by Martínez and Sanz⁵² and Sanz and Perales.⁵³ The influence of the rotation has been measured by Carruthers and Grasso;⁵⁴ Carruthers *et al.*;^{55,56} Tagg *et al.*;⁵⁷ Martínez;^{58,59} and Martínez and Meseguer.⁶⁰ The oscillatory behavior has been determined by Elagin, Levedev, and Tsmeliev;⁶¹ Sanz;²⁹ Martínez;⁵⁹ Martínez and Meseguer;⁶⁰ and Sanz and López-Diez.³³ On the other hand, some experimental works deal with the solidification process (Martínez *et al.*⁶²) and the influence of electrical fields (González *et al.*⁶³).

In this paper we present a theoretical analysis, based on the Cosserat model, of the response of viscous axisymmetric liquid bridges due to axial vibrations of the supporting disks. Although several studies related to the vibration of liquid bridges have been published, these studies are concerned mainly with the inviscid resonance frequencies. In addition, some attempts have been made to study the viscous case; however, the published analyses^{45,46} refer mainly to very long liquid bridges, $\Lambda \approx \pi$. Here the model used accounts for viscous liquid bridges with a wide range of slendernesses ($1 < \Lambda < \pi$). In addition, this model allows the calculation of not only resonance frequencies of such configurations, but also the frequency response of the liquid bridge. Finally, theoretical predictions are compared with experimental results obtained on Earth by using the neutral buoyancy technique, the experimental results being in good agreement with the theoretical ones.

To solve the problem a one-dimensional model has been used. This model is based on the one developed for capillary jet problems by Green,⁶⁴ which applies the basic theory of a one-dimensional Cosserat continuum. It has also been used in capillary jet problems by Bogy,⁶⁵⁻⁶⁸ and in liquid bridge problems by Meseguer³⁸ and Rivas and Meseguer.⁴⁶ It must be pointed out that although this model is equivalent to the Navier-Stokes equations in the limit $\Lambda \rightarrow \infty$, it is not consis-

tent with an asymptotic expansion of these equations in powers of Λ^{-1} (see Appendix A). Of course, it would have been preferable to develop a consistent expansion starting from an approach similar to lubrication theory but, unfortunately, the resulting system is too much complicated. Nevertheless, the model used has proven to give useful results that are in agreement with other much more complex models and with experimental results.

In the following, unless otherwise stated, all physical quantities are made dimensionless using the characteristic length R_0 and the characteristic time $(\rho R_0^3/\sigma)^{1/2}$.

II. PROBLEM FORMULATION

In carrying out the analysis the following assumptions are introduced: It is assumed that the properties of both the liquid (density and viscosity) and the interface (surface tension) are uniform and constant, and that the effects of the gas surrounding the liquid bridge are negligible. In addition, since only axisymmetric configurations are considered, the problem is assumed to be independent of the azimuthal coordinate. Under such assumptions the set of nondimensional differential equations and boundary conditions of the Cosserat model of the axisymmetric, nonrotating viscous flow are the following (Meseguer³⁸ and Rivas and Meseguer⁴⁶):

(a) continuity equation,

$$(F^2)_t + (F^2 W)_z = 0; \quad (1)$$

(b) axial momentum equation,

$$F^2 (W_t + W W_z) = -\mathcal{P}_z + (F^2)_z P_c + 2C (F^2 W_z)_z; \quad (2)$$

(c) radial momentum equation

$$\begin{aligned} \frac{1}{8} F^4 [(W_t + W W_z)_z - \frac{3}{2} W_z^2] \\ = -\mathcal{P} + F^2 P_c + \frac{1}{8} C [(F^4 W_{zz})_z - 8 F^2 W_z]. \end{aligned} \quad (3)$$

In these expressions $F(z,t)$ is the dimensionless equation of the liquid-gas interface and $W(z,t)$ the axial velocity at each plane parallel to the disks. Here \mathcal{P} is an arbitrary function of z and t , which will be removed from the formulation, whereas $P_c(z,t)$ accounts for both hydrostatic and capillary pressures, as explained in the following. The subscripts t and z indicate derivatives with respect to the time and the axial coordinate, respectively.

The formulation must be completed with boundary conditions: (i) the interface must remain anchored to the disk edges; and (ii) the axial velocity at each one of the disks must be equal to that of the corresponding supporting disks [which are assumed to be in a known position function of the time given by $z_1 = -\Lambda + \Lambda \lambda_1(t)$ and $z_2 = \Lambda + \Lambda \lambda_2(t)$]:

$$\begin{aligned} F[\Lambda + \Lambda \lambda_2(t), t] &= \frac{2}{1+K}, \\ F[-\Lambda + \Lambda \lambda_1(t), t] &= \frac{2K}{1+K}, \\ W[\Lambda + \Lambda \lambda_2(t), t] &= \Lambda \lambda_2'(t), \\ W[-\Lambda + \Lambda \lambda_1(t), t] &= \Lambda \lambda_1'(t), \end{aligned} \quad (4)$$

plus suitable initial conditions,

$$F(z,0) = F_i(z), \quad W(z,0) = W_i(z). \quad (5)$$

Equations (2) and (3) can be reduced to one single equation by elimination of \mathcal{D} between (2) and (3). If we choose as working variables $S = F^2$, which represents the cross-sectional area at z, t , and $Q = F^2 W$, which is proportional to the axial momentum of a slice, the above formulation becomes

$$S_t + Q_z = 0, \quad (6)$$

$$\begin{aligned} \mathcal{D}S - \frac{1}{8} \left\{ S^2 \left[\mathcal{D}_z - \frac{3}{2} \left(\frac{Q}{S} \right)_z \right] \right\}_z \\ = -SP_{c_z} - \frac{1}{8} C \left[S^2 \left(\frac{Q}{S} \right)_{zz} \right]_{zz} + 3C \left[S \left(\frac{Q}{S} \right)_z \right]_z, \end{aligned} \quad (7)$$

where

$$\mathcal{D} = [Q_t + (Q^2/S)_z]/S, \quad (8)$$

$$P_c = 4(2S + S_z^2 - SS_{zz})(4S + S_z^2)^{-3/2} + Bz. \quad (9)$$

Boundary conditions are now

$$\begin{aligned} S[\Lambda + \Lambda\lambda_2(t), t] &= \left(\frac{2}{1+K} \right)^2, \\ S[-\Lambda + \Lambda\lambda_1(t), t] &= \left(\frac{2K}{1+K} \right)^2, \\ Q[\Lambda + \Lambda\lambda_2(t), t] &= \Lambda\lambda_2'(t) \left(\frac{2}{1+K} \right)^2, \\ Q[-\Lambda + \Lambda\lambda_1(t), t] &= \Lambda\lambda_1'(t) \left(\frac{2K}{1+K} \right)^2, \end{aligned} \quad (10)$$

and initial conditions are

$$S(z,0) = S_i(z), \quad Q(z,0) = Q_i(z). \quad (11)$$

In addition, one more condition could be introduced stating the overall mass conservation during the evolution, that is

$$\pi \int_{-\Lambda + \Lambda\lambda_1(t)}^{\Lambda + \Lambda\lambda_2(t)} S(z,t) dz = V. \quad (12)$$

Concerning the above formulation it should be pointed out that boundary conditions must be fulfilled in two points whose position, although known, varies with time. To avoid the difficulties of this moving boundary condition a contraction of the axial coordinate is made and a new variable x is defined so that the interval of variation of the coordinate z (function of time) is mapped into a fixed interval. From the different possibilities, a simple linear mapping has been chosen:

$$x = x(z,t) = \Lambda \frac{z - g(t)}{\Lambda + h(t)} = \frac{z - g(t)}{1 + (1/\Lambda)h(t)}, \quad (13)$$

where

$$g(t) = \frac{\lambda_1(t) + \lambda_2(t)}{2} \Lambda, \quad (14)$$

gives the time variation of the position of the center of the liquid bridge (that point of the axis placed at every moment in the middle of the segment defined by the centers of the disks) and

$$h(t) = \frac{\lambda_2(t) - \lambda_1(t)}{2} \Lambda, \quad (15)$$

is the variation with time of the distance between the disks. In the coordinates x, t the disks are fixed, and their positions are given by

$$x[-\Lambda + \Lambda\lambda_1(t), t] = -\Lambda, \quad x[\Lambda + \Lambda\lambda_2(t), t] = \Lambda. \quad (16)$$

Using the new variable, the problem formulation now reads

$$S_t + x_t S_x + x_z Q_x = 0, \quad (17)$$

$$\begin{aligned} Q_t + x_t Q_x + x_z \left(\frac{Q^2}{S} \right)_x \\ - \frac{1}{8} x_z \left\{ S x_z \left[Q_t + x_t Q_x + x_z \left(\frac{Q^2}{S} \right)_x \right] \right. \\ \left. - S_x x_z \left[Q_t + x_t Q_x + x_z \left(\frac{Q^2}{S} \right)_x \right] - \frac{3}{2} S^2 x_z^2 \left(\frac{Q^2}{S} \right)_x \right\}_x \\ = -S x_z P_{c_x} - \frac{1}{8} C x_z^2 \left[S^2 x_z^2 \left(\frac{Q}{S} \right)_{xx} \right]_{xx} \\ + 3C x_z \left[S x_z \left(\frac{Q}{S} \right)_x \right]_x, \end{aligned} \quad (18)$$

$$P_c = 4(2S + x_z^2 S_x^2 - x_z^2 S S_{xx})(4S + x_z^2 S_x^2)^{-3/2} + Bx, \quad (19)$$

which must be solved with the boundary conditions

$$\begin{aligned} S(\Lambda, t) &= \left(\frac{2}{1+K} \right)^2, \quad S(-\Lambda, t) = \left(\frac{2K}{1+K} \right)^2, \\ Q(\Lambda, t) &= [g'(t) + h'(t)] \left(\frac{2}{1+K} \right)^2, \\ Q(-\Lambda, t) &= [g'(t) - h'(t)] \left(\frac{2K}{1+K} \right)^2, \end{aligned} \quad (20)$$

and the initial conditions

$$S(x,0) = S_i[z(x,0)], \quad Q(x,0) = Q_i[z(x,0)], \quad (21)$$

plus the condition of volume conservation,

$$\pi \int_{-\Lambda}^{\Lambda} S(x,t) \left(1 + \frac{1}{\Lambda} h(t) \right) dx = V. \quad (22)$$

If only small perturbations are considered [$g(t) \ll 1$ and $h(t) \ll 1$], the solution of the problem can be written as a static solution plus a small perturbation, i.e.,

$$\begin{aligned} S(x,t) &= S_0(x) + s(x,t), \\ Q(x,t) &= q(x,t), \\ P_c(x,t) &= P_0 + p(x,t). \end{aligned} \quad (23)$$

Then, the introduction of these expressions in (17)–(22), neglecting second-order terms, gives the following set of problems:

Zeroth-order problem:

$$4 \frac{2S_0 + S_{0x}^2 - S_0 S_{0xx}}{(4S_0 + S_{0x}^2)^{3/2}} + Bx = P_0, \quad (24)$$

$$S_0(\Lambda) = \left(\frac{2}{1+K} \right)^2, \quad S_0(-\Lambda) = \left(\frac{2K}{1+K} \right)^2, \quad (25)$$

$$\pi \int_{-\Lambda}^{\Lambda} S_0(x) dx = V; \quad (26)$$

first-order problem:

$$s_t + q_x = -x_t S_{0x}, \quad (27)$$

$$q_t - \frac{1}{8}(S_0 q_{tx} - S_{0x} q_t) = -S_0 p_x - \frac{1}{8} C \left[S_0^2 \left(\frac{q}{S_0} \right)_{xx} \right]_{xx} + 3C \left[S_0 \left(\frac{q}{S_0} \right)_x \right]_x, \quad (28)$$

$$p = 4(4S_0 + S_{0x}^2)^{-3/2} \left(2s + 2S_{0x} s_x - S_0 s_{xx} - s S_{0xx} - 2 \frac{h}{\Lambda} (S_{0x}^2 - S_0 S_{0xx}) \right) - 6(4S_0 + S_{0x}^2)^{-5/2} [2S_0 + S_{0x}^2 - S_0 S_{0xx}] \times \left(4s + 2S_0 s_x - 2 \frac{h}{\Lambda} S_{0x}^2 \right), \quad (29)$$

$$s(\pm \Lambda, t) = 0, \quad (30)$$

$$q(\pm \Lambda, t) = [g'(t) \pm h'(t)] S_0(\pm \Lambda), \quad (31)$$

$$s(x, 0) = S_t[z(x, 0)] - S_0(x), \quad q(x, 0) = Q_t[z(x, 0)], \quad (32)$$

$$\int_{-\Lambda}^{\Lambda} S_0(x) \frac{h(t)}{\Lambda} dx + \int_{-\Lambda}^{\Lambda} s(x, t) dx = 0. \quad (33)$$

Note that the zeroth-order problem consists on the determination of the equilibrium shape of a liquid bridge at rest, which can be solved with a method similar to the one used by Perales, Meseguer, and Martínez.²⁸

Concerning the first-order problem, the introduction of (29) into (28) allows the elimination of p . To eliminate $s(x, t)$ from the formulation, Eqs. (28) and (29) should be used simultaneously to formulate the problem in terms of $q(x, t)$, the resulting equation being

$$C_{41} q_{xxxxt} + C_{40} q_{xxxx} + C_{30} q_{xxx} + C_{22} q_{xxtt} + C_{21} q_{xxt} + C_{20} q_{xx} + C_{11} q_{xt} + C_{10} q_x + C_{02} q_{tt} + C_{01} q_t = C_{g1} g' + C_{h1} h', \quad (34)$$

where the functions C_{ij} depend on the capillary number, C , the slenderness, Λ , and the equilibrium shape, S_0 , and its derivatives with respect to x (additional details can be obtained upon request to the authors).

Equation (34) is fourth order in the variable x and, therefore, needs four boundary conditions to be solved. Two of them are given by Eq. (31) and the two remaining can be deduced from the boundary condition (30), which implies

$$s_t(\pm \Lambda, t) = 0, \quad (35)$$

and, substituting into Eq. (27), the two new boundary conditions are

$$q_x(\pm \Lambda, t) = [g' \pm h'] S_{0x}(\pm \Lambda). \quad (36)$$

From now on to solve the problem the following steps should be followed: (1) solve the zeroth-order problem given by Eq. (24) and boundary conditions (25) and (26). Let $S_0 = S_0(x)$ be the solution of the zeroth-order problem. (2) The zeroth-order solution $S_0 = S_0(x)$ is introduced into Eq. (34) and boundary conditions (31) and (36). By solving this problem $q = q(x, t)$ is obtained. (3) Once $q = q(x, t)$ is known, integration of Eq. (27) with respect to time allows

the calculation of $s = s(x, t)$. (4) Once $S_0(x)$, $s(x, t)$, and $q(x, t)$ are known, $S(x, t)$ and $Q(x, t)$ and therefore $S(z, t)$ and $Q(z, t)$ can be obtained from Eq. (23).

III. HARMONIC OSCILLATIONS OF A CYLINDRICAL-VOLUME LIQUID BRIDGE

The general formulation obtained in Sec. II has no apparent analytical solution, and it should be solved numerically (see Sec. IV). However, there is a case in which a simple analytical solution can be obtained; this occurs when the static equilibrium shape is that of a cylinder. This case is of great interest because, in spite of its simplicity, the simplified formulation maintains the qualitative behavior of the general problem.

It should be noted that the additional simplification of a cylindrical equilibrium shape implies that the supporting disks are equal in diameter ($K = 1$), zero gravity is assumed ($B = 0$) and that the volume of the liquid bridge is equal to that of a cylinder ($V = 2\pi\Lambda$). In this case the solution of the zeroth-order problem is $S_0(x) = 1$ and the first-order problem reduces to

$$s_t + q_x = 0, \quad (37)$$

$$q_t - \frac{1}{8} q_{txx} = -p_x - \frac{1}{8} C q_{xxxx} + 3C q_{xx}, \quad (38)$$

$$p_x = -\frac{1}{2} s_x - \frac{1}{2} s_{xxx}, \quad (39)$$

$$s(\pm \Lambda, t) = 0, \quad (40)$$

$$q(\pm \Lambda, t) = g'(t) \pm h'(t). \quad (41)$$

From the mass conservation Eq. (37), $q_x = -s_t$, and from boundary condition (40) the two additional boundary conditions for $q(x, t)$ are

$$q_x(\pm \Lambda, t) = 0. \quad (42)$$

Note that this formulation reduces to the slice model (Meseguer³⁸) by neglecting in Eq. (38) the term $-\frac{1}{8} q_{txx}$ (neglecting radial inertial effects) and setting $C = 0$ (neglecting viscosity effects).

By following a similar process to the one explained for the general formulation, the following equation is obtained:

$$q_{tt} - \frac{1}{8} q_{ttxx} + \frac{1}{2} q_{xx} + \frac{1}{2} q_{xxxx} + \frac{1}{8} C q_{txxxx} - 3C q_{txx} = 0, \quad (43)$$

which must be solved with the boundary conditions:

$$q(\pm \Lambda, t) = g'(t) \pm h'(t), \quad (44)$$

$$q_x(\pm \Lambda, t) = 0. \quad (45)$$

If a harmonic excitation $[g(t) = \text{Re}(Ge^{i\omega t}), h(t) = \text{Re}(He^{i\omega t})]$, where G and H are assumed to be real] is imposed the liquid bridge response can be written as

$$q(x, t) = \text{Re}[\mathcal{Q}(x)e^{i\omega t}], \quad (46)$$

where $\mathcal{Q}(x)$ is a complex function of the real variable x .

The substitution of these expressions in expressions (43)–(45) yields

$$(1 + \frac{1}{4} i\omega C) \mathcal{Q}_{xxxx} + (1 + \frac{1}{4} \omega^2 - 6i\omega C) \mathcal{Q}_{xx} - 2\omega^2 \mathcal{Q} = 0, \quad (47)$$

$$\mathcal{Q}(\pm \Lambda) = i\omega(G \pm H), \quad (48)$$

$$\mathcal{Q}_x(\pm \Lambda) = 0, \quad (49)$$

and then, if the solutions of this last problem are assumed to be of the form $\mathcal{Q}(x) = Ae^{\theta x}$, the following characteristic equation results:

$$(1 + \frac{1}{2}i\omega C)\theta^4 + (1 + \frac{1}{2}\omega^2 - 6i\omega C)\theta^2 - 2\omega^2 = 0, \quad (50)$$

whose roots are $\pm \theta_1, \pm \theta_2$,

$$\theta_1^2 = \frac{-1 - \frac{1}{2}\omega^2 + 6i\omega C}{2 + \frac{1}{2}i\omega C} + \frac{\sqrt{1 - 12i\omega C + \omega^2(\frac{1}{2} - 36C^2) - i\omega^3 C + \frac{1}{16}\omega^4}}{2 + \frac{1}{2}i\omega C}, \quad (51)$$

$$\theta_2^2 = \frac{-1 - \frac{1}{2}\omega^2 + 6i\omega C}{2 + \frac{1}{2}i\omega C} - \frac{\sqrt{1 - 12i\omega C + \omega^2(\frac{1}{2} - 36C^2) - i\omega^3 C + \frac{1}{16}\omega^4}}{2 + \frac{1}{2}i\omega C}. \quad (52)$$

Thus the solution of the problem is the linear combination of the four elementary solutions $\exp(\theta_1 x)$, $\exp(-\theta_1 x)$, $\exp(\theta_2 x)$, $\exp(-\theta_2 x)$, which fulfills the boundary conditions (48) and (49). It should be pointed out that the formulation of the problem is linear and thus superposition of solutions for the symmetric case (in phase oscillation of the disks $G \neq 0, H = 0$) and antisymmetric case (counterphase oscillation $G = 0, H \neq 0$) can be used.

Once $\mathcal{Q}(x)$ has been obtained, the evolution of the liquid bridge shape perturbation $s = s(x, t)$ can be obtained from the continuity equation. In effect, writing $s(x, t) = \text{Re}[\mathcal{S}(x)e^{i\omega t}]$, where $\mathcal{S}(x)$ is a complex function of the real variable x , from Eq. (37) one obtains

$$\mathcal{S}(x) = -(1/i\omega)\mathcal{Q}_x. \quad (53)$$

The final results as a function of the roots of the characteristic equation, (51) and (52), are

$$\mathcal{Q}(x) = i\omega G \frac{\theta_2 \sinh \theta_2 \Lambda \cosh \theta_1 x - \theta_1 \sinh \theta_1 \Lambda \cosh \theta_2 x}{\theta_2 \sinh \theta_2 \Lambda \cosh \theta_1 \Lambda - \theta_1 \sinh \theta_1 \Lambda \cosh \theta_2 \Lambda} + i\omega H \frac{\theta_2 \cosh \theta_2 \Lambda \sinh \theta_1 x - \theta_1 \cosh \theta_1 \Lambda \sinh \theta_2 x}{\theta_2 \cosh \theta_2 \Lambda \sinh \theta_1 \Lambda - \theta_1 \cosh \theta_1 \Lambda \sinh \theta_2 \Lambda}, \quad (54)$$

$$\mathcal{S}(x) = -G\theta_1\theta_2 \frac{\sinh \theta_2 \Lambda \sinh \theta_1 x - \sinh \theta_1 \Lambda \sinh \theta_2 x}{\theta_2 \sinh \theta_2 \Lambda \cosh \theta_1 \Lambda - \theta_1 \sinh \theta_1 \Lambda \cosh \theta_2 \Lambda} - H\theta_1\theta_2 \frac{\cosh \theta_2 \Lambda \cosh \theta_1 x - \cosh \theta_1 \Lambda \cosh \theta_2 x}{\theta_2 \cosh \theta_2 \Lambda \sinh \theta_1 \Lambda - \theta_1 \cosh \theta_1 \Lambda \sinh \theta_2 \Lambda}. \quad (55)$$

The response due to a symmetric excitation (in-phase oscillation of the disks $G \neq 0, H = 0$) is antisymmetric in the liquid bridge shape (with respect to $x = 0$), whereas the antisymmetric excitation (counterphase oscillation $G = 0, H \neq 0$) gives a symmetric response of the shape.

Note that although the conservation of volume [Eq. (33)] has not been explicitly imposed, it should be pointed out that it is automatically fulfilled [due to the fulfillment of the local conservation of mass, Eq. (37)].

It could be of interest to compare the behavior of the liquid bridge response for low frequencies with the static behavior predicted by other authors. Following Meseguer,¹⁵ the deformation of the liquid bridge interface when the liquid bridge volume is not that of a cylinder, or when a small residual axial gravity is considered, is given by

$$S(x, t) = 1 + \left(\frac{V}{2\pi\Lambda} - 1\right)\Lambda \frac{\cos x - \cos \Lambda}{\sin \Lambda - \Lambda \cos \Lambda} + 2B\left(x - \Lambda \frac{\sin x}{\sin \Lambda}\right). \quad (56)$$

To compare our results with (56) it must be considered that, in the present model, the roots of the characteristic equation can be approximated, when excitation frequencies are small enough, $\omega \rightarrow 0$, by the expressions

$$\theta_1 = \pm \sqrt{2}\omega + O(\omega^2), \quad (57)$$

$$\theta_2 = \pm i + O(\omega), \quad (58)$$

and in this case the antisymmetric and symmetric parts of the response are, respectively,

$$\mathcal{S}(x) = -2\omega^2 G \left(x - \Lambda \frac{\sin x}{\sin \Lambda}\right) + O(\omega^3), \quad (59)$$

$$\mathcal{S}(x) = -H \frac{\cos x - \cos \Lambda}{\sin \Lambda - \Lambda \cos \Lambda} + O(\omega). \quad (60)$$

To compare Eq. (59) with Eq. (56) it must be taken into account that an in-phase oscillation of the disks ($G \neq 0, H = 0$) can be reduced to a problem in which the positions of the disks remain constant with time by changing the origin of the coordinate system to the point $x_0 = g(t)$, but in this case inertia forces given by $\ddot{x}(t) = -\omega^2 \text{Re}(Ge^{i\omega t})$ must be added. This is equivalent to considering that liquid bridge is excited by an oscillatory gravitational field with an intensity $B(t) = \text{Re}(Be^{i\omega t})$, so that in the limit $\omega \rightarrow 0$, Eq. (59) can be written as

$$\mathcal{S}(x) = 2B\left(x - \Lambda \frac{\sin x}{\sin \Lambda}\right), \quad (61)$$

which is similar to Eq. (56) in the case of cylindrical volume.

To compare volume effects in the equilibrium shape it must be observed that the liquid bridge response due to an antisymmetric excitation corresponds to a change in slenderness, $\Lambda_e(t) = \Lambda + \text{Re}(He^{i\omega t})$, without change of volume (oscillatory stretching) and following Meseguer,¹⁵

$$S(x,t) = 1 + \left(\frac{2\pi\Lambda}{2\pi} - \Lambda_e(t) \right) \frac{\cos x - \cos \Lambda_e(t)}{\sin \Lambda_e(t) - \Lambda_e(t) \cos \Lambda_e(t)} \quad (62)$$

This last expression can be approximated, in the case $H \ll 1$, by

$$S(x,t) = 1 - \operatorname{Re}(He^{i\omega t}) \frac{\cos x - \cos \Lambda}{\sin \Lambda - \Lambda \cos \Lambda}, \quad (63)$$

which coincides with Eq. (56) when $B = 0$.

To estimate the accuracy of the Cosserat model the results obtained have been compared (Fig. 2) with those given by other models. Thus the first resonance frequency (the lowest frequency for which a maximum in the response, or an infinity if zero viscosity is assumed, appears) has been computed using the present model and the one-dimensional slice model of Meseguer³⁸ and the three-dimensional model of Sanz²⁹ (in the last case the influence of the outer bath has been neglected). In order to compare them, zero viscosity has been considered ($C = 0$) in the Cosserat model. Results here obtained are in agreement with those of Sanz²⁹ up to values of the slenderness below $\Lambda = 1$, the differences increasing as Λ decreases, whereas the one-dimensional slice model is only valid for $\Lambda > 2$. The differences between Cosserat and slice model (both are one-dimensional models) are due to the radial momentum terms, which in the slice model are completely neglected, which are of importance when the slenderness of the liquid bridge is not too high.

In the following plots the liquid bridge response versus the frequency of the perturbation (transfer function) has been represented when subjected to several excitations. The liquid bridge response has been defined as in Meseguer,⁴¹ as the ratio of the maximum interface deformation of the liquid bridge, in each cycle, to the amplitude of the perturbation.

According to this definition, in Figs. 3–5 the liquid bridge response has been represented when both disks are

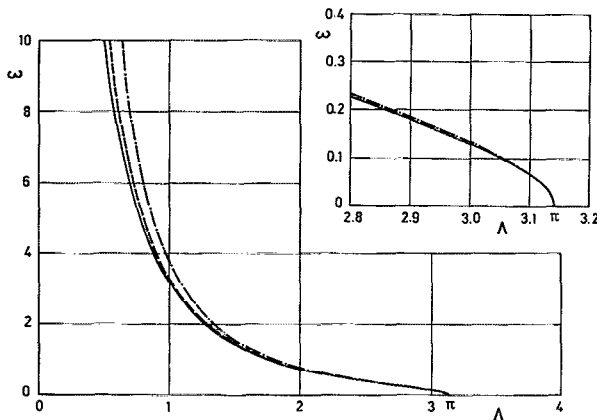


FIG. 2. Variation with the slenderness, Λ , of the dimensionless pulsation, ω , corresponding to the first oscillation mode of inviscid liquid bridges between equal disks, $K = 1$, with cylindrical volume, $V = 2\pi\Lambda$, and in gravitationless conditions, $B = 0$. Line type indicates the mathematical model according to the following key: —, one-dimensional Cosserat model; ---, three-dimensional model (Sanz²⁹); - · -, one-dimensional slice model (Meseguer³⁸).

vibrating in phase (Fig. 3), when they are 180° out of phase (Fig. 4), and when only one of the disks is oscillating (Fig. 5).

Concerning the first of the three plots, it should be pointed out that the liquid bridge response becomes zero when ω is small enough [the response is proportional to ω^2 , see Eq. (59)], whereas for large values of ω the response is of order of unity (except in the resonances, where it is much larger). In the counterphase case the behavior at low values of ω is rather different. As $\omega \rightarrow 0$ the liquid bridge response becomes equal to a constant value [different from zero; see Eq. (60)] because of the reason already stated: at low frequencies it can be assumed that the liquid bridge evolution is a quasistatic evolution, in which the liquid bridge interface is defined by the static equilibrium shape corresponding to the given volume and a slenderness that varies with time according to the separation between both disks.

Note also that frequencies of resonance in Fig. 4 are rather different from those appearing in Fig. 3. The reason for this difference is that an in-phase excitation (which is a symmetric perturbation in respect to the plane $x = 0$) causes an antisymmetric response (in respect to $x = 0$), whereas the contrary occurs in the counterphase case. Therefore, in the in-phase case only antisymmetric oscillation modes are excited and when the disks are oscillating in counterphase

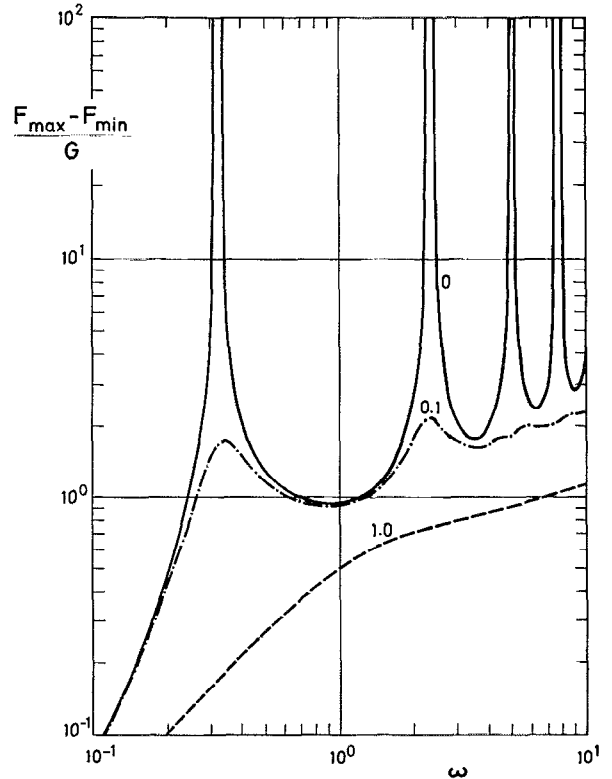


FIG. 3. Transfer function of a liquid bridge between equal disks, $K = 1$, slenderness $\Lambda = 2.6$, cylindrical volume, $V = 2\pi\Lambda$, and in gravitationless conditions, $B = 0$, when subjected to an in-phase vibration of the supporting disks ($G \neq 0$, $H = 0$). Numbers on the curves indicate the value of the viscosity parameter, C .

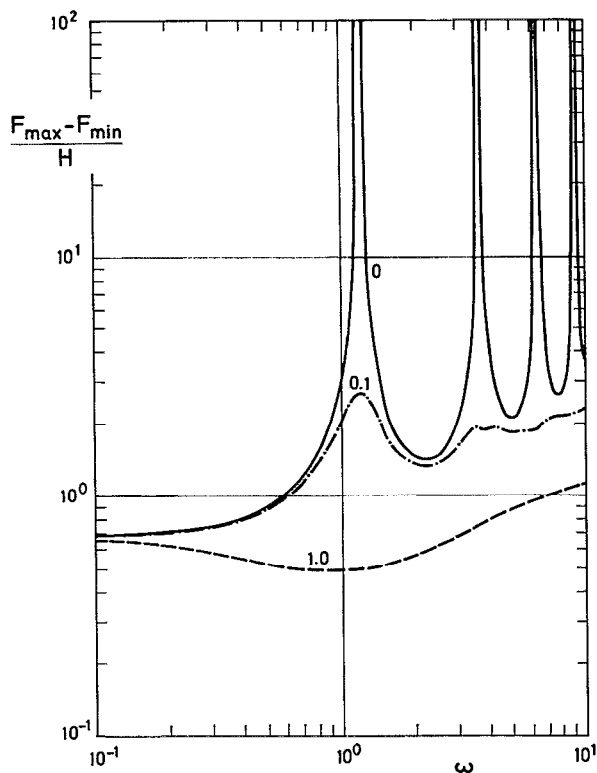


FIG. 4. Transfer function of a liquid bridge between equal disks, $K = 1$, slenderness $\Lambda = 2.6$, cylindrical volume, $V = 2\pi\Lambda$, and in gravitationless conditions, $B = 0$, when subjected to an in-counterphase vibration of the supporting disks ($G = 0$, $H \neq 0$). Numbers on the curves indicate the value of the viscosity parameter, C .

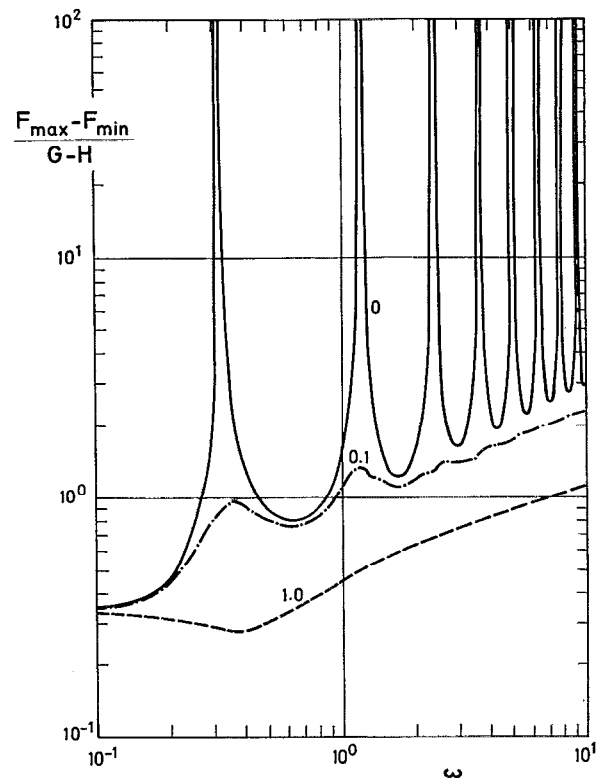


FIG. 5. Transfer function of a liquid bridge between equal disks, $K = 1$, slenderness $\Lambda = 2.6$, cylindrical volume, $V = 2\pi\Lambda$, and in gravitationless conditions, $B = 0$, when subjected to a vibration of one of the supporting disks ($G = -H \neq 0$). Numbers on the curves indicate the value of the viscosity parameter, C .

the only resonances appearing are those corresponding to symmetric oscillation modes (this behavior will be the same provided the liquid bridge configuration is symmetric with respect to $x = 0$, which means $K = 1$ and $B = 0$ no matter what the value of V is). Note that for the selected value $\Lambda = 2.6$ the value $C = 1$ is over the critical value (no resonances appear).

The third perturbation considered has been the vibration of one of the disks, whereas the opposite one is kept at rest (Fig. 5) or, in other words, $G = -H = a/2$. This perturbation is the one usually used in experiments, and in this case both symmetric and nonsymmetric oscillation modes appear.

To compare with the results presented in Meseguer,⁴¹ obtained by using a one-dimensional slice model, in Fig. 6 the response of a liquid bridge subjected to an oscillatory microgravitational field has been plotted [$B(t) = \text{Re}(B_0 e^{i\omega t})$, where $B_0 = -\omega^2 G$]. In this case the liquid bridge response has a nonzero value when $\omega \rightarrow 0$ [which is the static deformation of the interface when an axial Bond number is considered, Eq. (61)] and when ω is large, except at the resonances, the transfer function varies as ω^{-2} . The behavior predicted by both models (slices and Cosserat) is similar, although the values of the frequencies of resonance predicted by the slice model are greater than those predicted

by the Cosserat one, the differences increasing as ω increases.

An interesting phenomenon widely used in experimentation is that at resonances the phase shift between the perturbation and the response is $\pi/2$. The phase shift between the perturbation and liquid bridge response has been represented in Fig. 7. In this case the transfer function has been defined as the variation along a cycle of the interface radius at selected sections ($z = -\Lambda/2, 0, \Lambda/2$). As it can be observed, the phase shift is $\pi/2$ at the points where the transfer function is maximum (resonances), but it can be also observed that there are, depending on the considered section, some values of ω in which the phase shift is $\pi/2$ but they do not correspond to resonances. This effect should be carefully taken into account if it would be desired to design some device to automatically detect resonances based only on phase shift measurements.

To evaluate the influence of viscosity on the response of liquid bridges the attention has been focused mainly on the resonance corresponding to the first oscillation mode of liquid bridges subjected to an in-phase oscillation of the supporting disks. In Fig. 8 the variation with the viscosity parameter C of the pulsation of resonance, ω , has been plotted. As shown in the figure, as C increases ω increases, but for each value of Λ , there is a value of C beyond which the maxi-

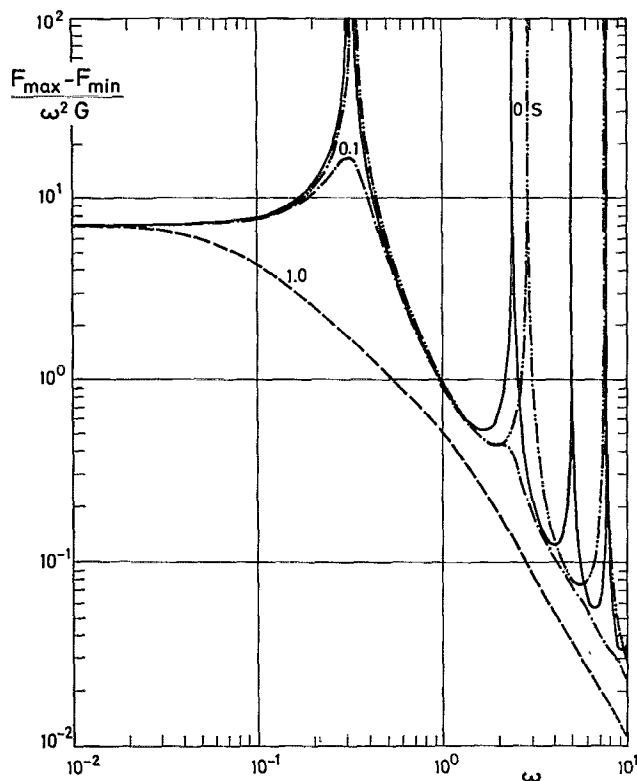


FIG. 6. Transfer function of a liquid bridge between equal disks, $K = 1$, slenderness $\Lambda = 2.6$, cylindrical volume, $V = 2\pi\Lambda$, when subjected to an oscillatory microgravitational field, $B(t) = \text{Re}(-\omega^2 G e^{i\omega t})$. Numbers on the curves indicate the value of the viscosity parameter, C . The line S indicates results from the inviscid one-dimensional slice model.

imum in the response curve disappears, this value of C corresponding to the critical damping for the chosen slenderness. This critical value of C increases as Λ decreases, which means that a small value of viscosity could prevent detection of resonances if the liquid bridge slenderness were large

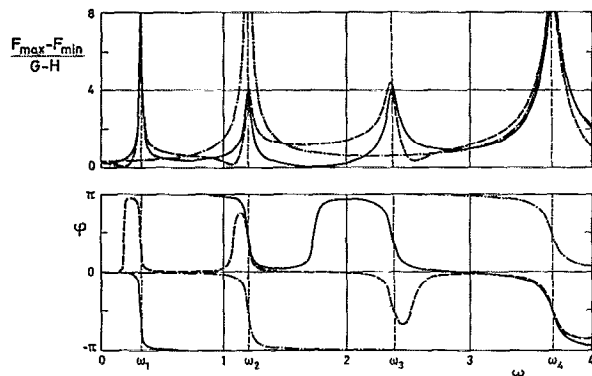


FIG. 7. Transfer function and phase shift, φ , between the perturbation and the liquid bridge response at selected sections. The results correspond to the following liquid bridge configuration: $\Lambda = 2.6$, $V = 2\pi\Lambda$, $K = 1$, $B = 0$, $C = 0.01$. Line type indicates the different sections of the liquid bridge according to the following key: —, $z = -\Lambda/2$; ---, $z = 0$; and - · -, $z = \Lambda/2$.

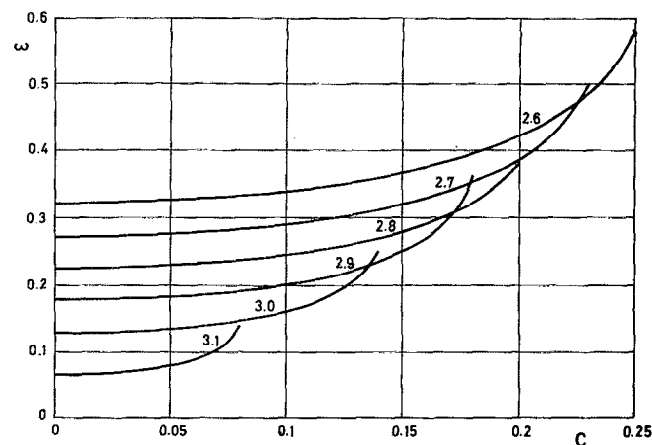


FIG. 8. Dependence on the viscosity parameter, C , of the pulsation of resonance corresponding to the first oscillation mode, ω , of liquid bridges with $K = 1$, $B = 0$, and $V = 2\pi\Lambda$. Numbers on the curves indicate the value of the slenderness, Λ .

enough. Another important effect due to viscosity is the decreasing of the maximum of the liquid bridge response at resonance (Fig. 9).

Finally, it should be pointed out that this Cosserat model reproduces an experimental behavior, which can be observed when the exciting frequency is high enough. In such case only a small region of the liquid column, that close to the oscillating disk, is perturbed. If ω is high enough the roots of the characteristic equation can be written as

$$\begin{aligned}\theta_1 &\approx \pm 2\sqrt{2}, \\ \theta_2 &\approx \pm \omega \left(\frac{-4 + i\omega C}{16 + \omega^2 C^2} \right)^{1/2},\end{aligned}\quad (64)$$

and then, also taking into account that $\theta_2 \gg \theta_1$, the following simplified expression for the liquid bridge interface results: in phase oscillation of the supporting disks,

$$\mathcal{S}(x) = -2\sqrt{2}G \frac{\sinh \theta_1 \Lambda}{\cosh \theta_1 \Lambda} \left(\frac{\sinh \theta_1 x}{\sinh \theta_1 \Lambda} - \frac{\sinh \theta_2 x}{\sinh \theta_2 \Lambda} \right), \quad (65)$$

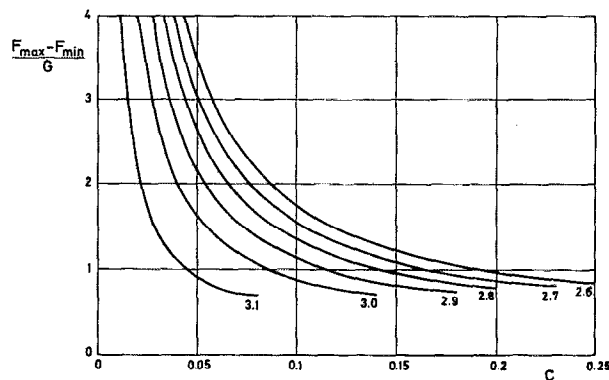


FIG. 9. Dependence on the viscosity parameter, C , of the liquid bridge response at the first resonance. The results correspond to the following liquid bridge configuration: $K = 1$, $B = 0$, $V = 2\pi\Lambda$. Numbers on the curves indicate the value of the slenderness, Λ .

counterphase oscillation of the supporting disks,

$$\mathcal{S}(x) = -2\sqrt{2}H \frac{\cosh \theta_1 \Lambda}{\sinh \theta_1 \Lambda} \left(\frac{\cosh \theta_1 x}{\cosh \theta_1 \Lambda} - \frac{\cosh \theta_2 x}{\cosh \theta_2 \Lambda} \right). \quad (66)$$

According to these expressions the wave number of the interface deformation is $\text{Im}(\theta_2)$ and such interface deformation disappears at a distance of the order of $1/\text{Re}(\theta_2)$ from the oscillatory disk. The interface deformation of a typical configuration is shown in Fig. 10. Observe that in this plot only the half of the liquid bridge interface (that close to the oscillating side) has been plotted.

IV. FORCED OSCILLATION OF A GENERAL-CONFIGURATION LIQUID BRIDGE

The dynamics of general-configuration liquid bridge ($K \neq 1$, $B \neq 0$, $V \neq 2\pi\Lambda$) has been solved through a finite-difference method, similar to the one used by Meseguer⁴¹ to solve the slice model in the case of an inviscid liquid bridge subjected to an oscillatory axial microgravity field.

In the following it is assumed that both the liquid bridge perturbation, $g(t)$ and $h(t)$, and the liquid bridge response, $q(x,t)$ and $s(x,t)$, are harmonic functions of time, i.e.,

$$\begin{aligned} g(t) &= \text{Re}(Ge^{i\omega t}), \\ h(t) &= \text{Re}(He^{i\omega t}), \\ q(x,t) &= \text{Re}[\mathcal{Q}(x)e^{i\omega t}], \\ s(x,t) &= \text{Re}[\mathcal{S}(x)e^{i\omega t}], \end{aligned} \quad (67)$$

where G and H are real constants, whereas $\mathcal{Q}(x)$ and $\mathcal{S}(x)$ are complex functions of the real variable x . After introduction of these expressions in Eqs. (27) and (34) and boundary conditions (31) and (36) the following problem results:

$$C_4(x)\mathcal{Q}_{xxxx} + C_3(x)\mathcal{Q}_{xxx} + C_2(x)\mathcal{Q}_{xx} + C_1(x)\mathcal{Q}_x + C_0(x)\mathcal{Q} = C_g(x)G + C_h(x)H, \quad (68)$$

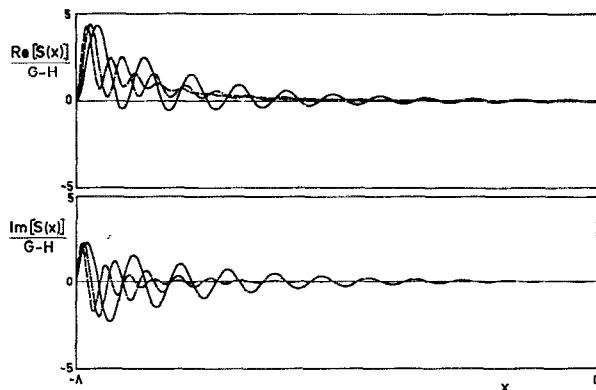


FIG. 10. Variation with the reduced axial coordinate, x , of both the real and imaginary parts of the function defining the liquid bridge interface shape, $\mathcal{S}(x)$, when subjected to high-frequency oscillation of the disk placed at $x = -\Lambda$. The results correspond to a liquid bridge with $\Lambda = 2.8$, $V = 2\pi\Lambda$, $K = 1$, $B = 0$, and $C = 0.01$. Line type indicates the value of the pulsation according to the following key: —, $\omega = 50$; - - -, $\omega = 75$; and - · -, $\omega = 100$.

$$\mathcal{Q}(\pm\Lambda) = i\omega(G \pm H)S_0(\pm\Lambda), \quad (69)$$

$$\mathcal{Q}_x(\pm\Lambda) = i\omega(G \pm H)S_{0x}(\pm\Lambda), \quad (70)$$

$$\mathcal{S}(x) = i\omega\mathcal{Q}_x + \left(G + \frac{x}{\Lambda}H\right)S_{0x}. \quad (71)$$

where $C_i(x)$ are complex functions of the real variable x , and of C_{41} , C_{40} , C_{30} , C_{22} , C_{21} , C_{20} , C_{11} , C_{10} , C_{01} , C_{g1} , and C_{h1} , which are real functions of x .

To solve the above formulation an implicit finite-difference method is used, with a centered five-point scheme for the evaluation of the spatial derivatives (Fig. 11),

$$x_j = -\Lambda + 2\Lambda(j/n), \quad j = -2, \dots, n+2,$$

$$\mathcal{Q}_j = \mathcal{Q}(x_j),$$

$$\mathcal{Q}_{xj} = \frac{[8(\mathcal{Q}_{j+1} - \mathcal{Q}_{j-1}) - \mathcal{Q}_{j+2} + \mathcal{Q}_{j-2}]}{12\delta},$$

$$\begin{aligned} \mathcal{Q}_{xxj} &= \frac{[16(\mathcal{Q}_{j+1} + \mathcal{Q}_{j-1}) - \mathcal{Q}_{j+2} - \mathcal{Q}_{j-2} - 30\mathcal{Q}_j]}{12\delta^2}, \\ \mathcal{Q}_{xxxj} &= \frac{[-2(\mathcal{Q}_{j+1} - \mathcal{Q}_{j-1}) + \mathcal{Q}_{j+2} - \mathcal{Q}_{j-2}]}{2\delta^3}, \end{aligned}$$

$$\begin{aligned} \mathcal{Q}_{xxxxj} &= \frac{[-4(\mathcal{Q}_{j+1} + \mathcal{Q}_{j-1}) + \mathcal{Q}_{j+2} + \mathcal{Q}_{j-2} + 6\mathcal{Q}_j]}{\delta^4}, \end{aligned} \quad (72)$$

with $\delta = 2\Lambda/n$, n being the number of equally spaced nodes in the grid. Two external spurious values at each side ($j = -2, -1, n+1, n+2$) have been introduced in order to keep the same centered scheme for all points. Substitution of (72) in the problem formulation gives $n+1$ equations:

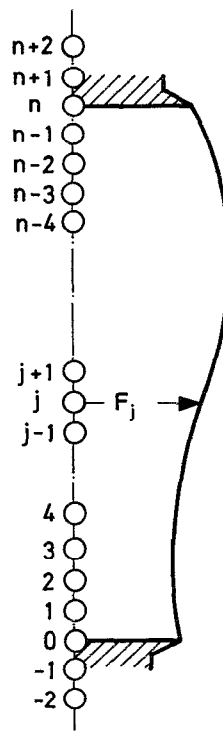


FIG. 11. Sketch of the spatial grid used in computations.

$$A_{jj-2}\mathcal{Q}_{j-2} + A_{jj-1}\mathcal{Q}_{j-1} + A_{jj}\mathcal{Q}_j + A_{jj+1}\mathcal{Q}_{j+1} + A_{jj+2}\mathcal{Q}_{j+2} = B_j, \quad j = 0, \dots, n, \quad (73)$$

plus four additional equations, which are obtained from boundary conditions,

$$\begin{aligned} \mathcal{Q}_0 &= i\omega(G - H)S_0(-\Lambda), \\ \mathcal{Q}_n &= i\omega(G + H)S_0(\Lambda), \\ \mathcal{Q}_{x_0} &= \frac{8(\mathcal{Q}_1 - \mathcal{Q}_{-1}) - \mathcal{Q}_2 + \mathcal{Q}_{-2}}{12\delta} \\ &= i\omega(G - H)S_{0x}(-\Lambda), \\ \mathcal{Q}_{x_n} &= \frac{8(\mathcal{Q}_{n+1} - \mathcal{Q}_{n-1}) - \mathcal{Q}_{n+2} + \mathcal{Q}_{n-2}}{12\delta} \\ &= i\omega(G + H)S_{0x}(\Lambda). \end{aligned} \quad (74)$$

Therefore, there is a system of $n + 5$ equations that allows the calculation of the $n + 5$ unknowns \mathcal{Q}_j ($j = -2, \dots, n + 2$).

This system of equations can be written in a more compact form as

$$[A]\{\mathcal{Q}\} = \{B\} \Rightarrow \{\mathcal{Q}\} = [A]^{-1}\{B\}. \quad (76)$$

Once \mathcal{Q}_j is known at $j = -2, \dots, n + 2$ [note that (76) must be computed using complex algebra] \mathcal{S}_j can be calculated at $j = 0, \dots, n$ through the continuity equation

$$\mathcal{S}(x_j) = i\omega\mathcal{Q}_{xj} + \left(G + \frac{x_j}{\Lambda}H\right)S_{0x}(x_j). \quad (77)$$

It should be pointed out that prior to the solution of the problem of the dynamics it is necessary to calculate the static equilibrium shape $S_0(x_j)$, since this equilibrium shape appears in the terms of matrix $[A]$ as well as in the vector $\{B\}$ (additional details on the numerical method can be obtained upon request to the authors).

Before the results obtained are presented, it would be convenient to make some comments on the accuracy of the numerical computation. A typical feature of problems where surface-tension effects are present is the high order of the spatial derivatives involved (in our particular case, these derivatives have been calculated through a five-point scheme). Leaving aside the fact that the order of the approximation in the numerical evaluation of derivatives decreases as the order of differentiation increases, there is a source of error associated with the five-point scheme used, which arises when these derivatives are evaluated close to the boundary points. In effect, this scheme introduces four outer points (two external points at each disk) in which the values of \mathcal{Q} must be calculated to fulfill boundary conditions. Since these outer values, which have no physical meaning, affect some terms of the matrix $[A]$, they introduce some spurious information in calculations, whose effect decreases with the size δ of the spatial grid. Therefore the first computations have been performed, aiming at establishing the optimum of this grid size, solving a test case ($\Lambda = 2.6$, $V = 2\pi\Lambda$, $C = 0$, $B = 0$, $K = 1$) several times, varying each time the number of steps n between the disks, and comparing the results obtained with the exact solution (note that the selected case may be solved by

using the model presented in Sec. III). The results obtained are plotted in Fig. 12, which shows that the first resonance pulsation ω increases with n , but the rate of increase tends to zero for large values of n (the slope is practically zero at $n = 60$). The variation with n of the needed computation time, which increases potentially with n , is also presented in this plot. Therefore choosing a value for n is a tradeoff between accuracy and computing time. For all the computations from now on the value $n = 40$ has been used; this value gives, according to Fig. 12, a resonance frequency already 99.5% of that obtained from the exact solution, whereas computing time is more than three times smaller than the one needed if $n = 60$ is chosen.

Although this model allows one to analyze the dependence of the liquid bridge oscillation on multiple parameters (Λ , V , K , C , B , ω , G , and H), the results presented in the following mainly concern the effect on the solution of some of them (V , K , and B) since the effect of the remainder have been already analyzed in Sec. III. It has also been assumed that the oscillation of both supporting disks are in phase and the analysis has been limited to the first frequency of resonance.

First of all, the results obtained with this model (particularly the influence of volume on the first oscillation mode) are compared with those obtained by Gañán³² by using a three-dimensional inviscid model, and by Meseguer⁴¹ through a one-dimensional inviscid slice model (Fig. 13). Since these two last models are inviscid, in calculations it has been assumed that $C = 0$. According to this plot the agreement between three-dimensional results and that obtained with the Cosserat model is very good, even for a slenderness as low as $\Lambda = 1.6$ (which is the smaller value considered in Gañán³²).

The influence of volume and viscosity on the first frequency of resonance is shown in Fig. 14. As it can be observed, ω increases as C increases, and there is also a critical damping. In this plot it is shown that close to the critical damping ω increases slightly as V decreases. This phenomenon can be explained by plotting the transfer function of

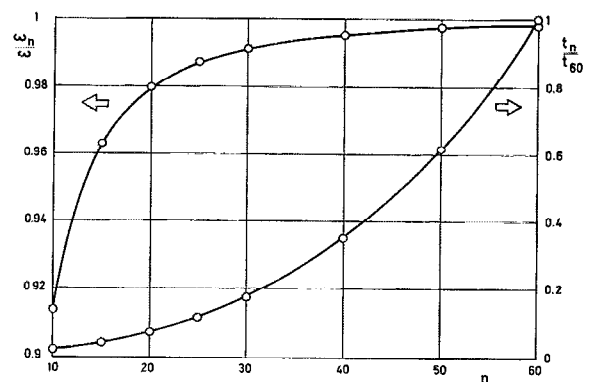


FIG. 12. Variation with the number of points of the spatial grid, n , of the first pulsation of resonance, ω_n , divided by the value obtained analytically through the simplified model presented in Sec. III, ω , and the computing time, t_n , divided by the computing time needed for $n = 60$. The results correspond to a liquid bridge with $\Lambda = 2.6$, $V = 2\pi\Lambda$, $K = 1$, $B = 0$, and $C = 0$.

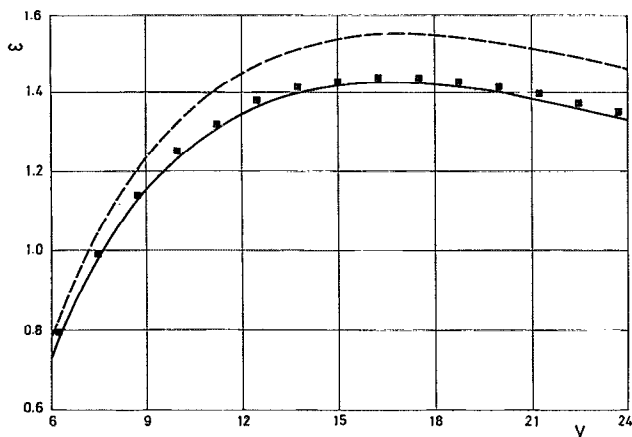


FIG. 13. Variation with the volume, V , of the first pulsation of resonance, ω , of a liquid bridge with $\Lambda = 1.6$, $K = 1$, $B = 0$, and $C = 0$. Line type indicates results obtained from the Cosserat model (continuous line) or the slice model (dashed line). The closed symbols indicate results from the three-dimensional inviscid model developed by Gafán (Ref. 32).

liquid bridges having volumes close enough to that of the critical damping, as shown in Fig. 15. In this plot it can be observed that the values of ω corresponding to the first resonance (which are those corresponding to the maxima of the transfer functions) decrease as V decreases, except in the vicinity of the critical damping, where ω increases (beyond the critical damping the transfer function has no maximum).

Finally, in Fig. 16 the variation with Bond number, B , of the first frequency of resonance of a liquid bridge with $\Lambda = 2.4$, $V = 16.0$, $K = 0.7$, and $C = 0$ has been represented. Note that ω is zero for $B = -0.0056$ and becomes zero again at $B = 0.2067$. This behavior is explained because of minimum volume stability limits. In effect, when disks are unequal in radius, for selected values of Λ and V , there are

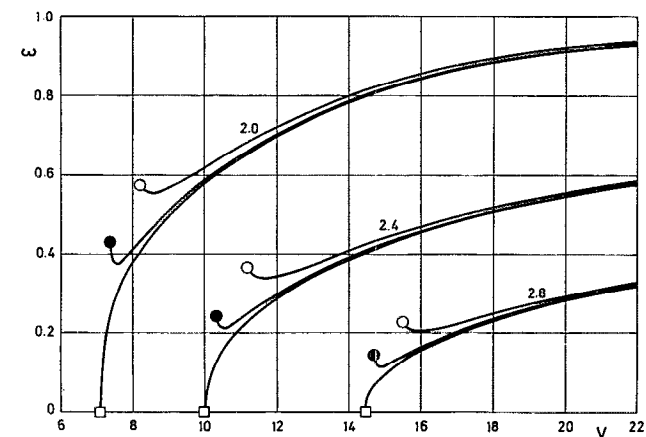


FIG. 14. Variation with the volume, V , of the first pulsation of resonance, ω , of liquid bridges with $K = 1$ and $B = 0$. Numbers on the curves indicate the value of the slenderness, whereas the symbols identify the value of the viscosity parameter according to the following key: \square , $C = 0$; \bullet , $C = 0.05$; \circ , $C = 0.1$.

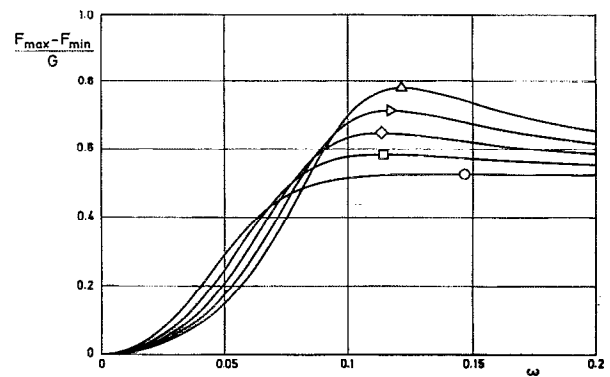


FIG. 15. Transfer function of a liquid bridge with $\Lambda = 2.8$, $K = 1$, $B = 0$, and $C = 0.05$ when subjected to an in-phase vibration of the supporting disks ($G \neq 0$, $H = 0$). The symbols are placed at the maximum of each one of the curves and the value of the dimensionless volume, V , is identified according to the following key: \circ , $V = 14.7$; \square , $V = 14.8$; \diamond , $V = 14.9$; \triangleright , $V = 15.0$; Δ , $V = 15.1$.

two values of B for which the liquid bridge becomes unstable (Meseguer *et al.*¹⁸ and Perales *et al.*²⁸), these values of B being those for which $\omega = 0$. The behavior shown in Fig. 16 is rather different of that shown in Fig. 13; in that plot ω decreases with V beyond the maximum, but the curve does not end at $\omega = 0$ but at some value $\omega \neq 0$ (as V increases the liquid bridge behavior becomes similar to that of a drop). On the other hand, in Fig. 16 the curve ends at $\omega = 0$, the reason being, as already explained, that as B increases a second minimum volume stability limit is reached.

V. EXPERIMENTAL RESULTS

A problem arising when experiments with axisymmetric liquid bridges of general configuration are performed is the large number of parameters involved. These parameters are the slenderness of the liquid bridge, Λ , the dimensionless volume of liquid, V , the ratio of the lower disk radius to the upper disk radius, K , the Bond number, B , the viscosity pa-

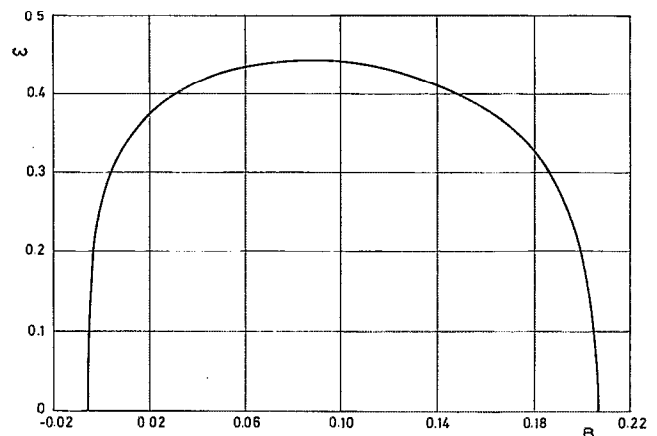


FIG. 16. Variation with the Bond number, B , of the first pulsation of resonance, ω , of a liquid bridge with $\Lambda = 2.4$, $V = 16$, $K = 0.7$, and $C = 0$.

parameter, C , and the dimensionless amplitude and frequency of disks oscillation. Therefore, in order to maintain the experimental effort within reasonable limits, some selection of the values of the above-mentioned parameters is needed. In the experiments described in the following only liquid bridges between equal disks ($K = 1$) have been used.

Experiments have been performed in an apparatus called Tele-Operated Plateau Tank (TOPT) Facility already described by Sanz-Andrés *et al.*⁶⁹ The working configuration consists of a column of silicone oil (with kinematic viscosity $\nu = 10^{-5} \text{ m}^2 \text{ sec}^{-1}$ and density $\rho = 936 \text{ kg m}^{-3}$) placed vertically inside a mixture of methanol and water of almost the same density of the silicone oil. The overall arrangement, as sketched in Fig. 17, consists of a tank that contains the methanol-water mixture and the liquid bridge held between two coaxial disks. Both disks are made of Perspex, in the shape of a frustum cone, to provide sharp edges, their diameter being 30 mm ($K = 1$). The injection and removal of working fluid is done through a 4 mm diam hole in the center of the upper disk. The working surface of the bottom disk is flat, whereas the one of the feeding disk presents a slight conicity, the purpose of which is to facilitate the evacuation through the injection hole of the air bubbles trapped in the liquid bridge. Working fluid injection and removal is done with a calibrated syringe, the piston of which is driven by a variable speed motor. Liquid displaced by the piston passes through the filling duct in which a three-way valve with a purge duct is connected aiming to trap air bubbles coming from the upper disk.

Background illumination consists of a 150 W fiber optic illuminator (similar to those used in microscopy). A CCD video camera, placed 1 m away, is used for image recording. To enhance the visualization of the shape of the liquid bridge (outline of its free surface) only one-half of the background illumination plane is illuminated. This type of illumination has been used because it allows the tracking of the interface, even if the bridge breaks into two drops. Automated image analysis has been developed, so that the liquid contour can be extracted in near real time from the video frames.

Prior to the description and analysis of the experiments on the dynamic response of axisymmetric liquid bridges, a

set of previous tests will be presented. These previous tests concern the measurement of the surface tension between the fluid of the liquid column and the outer bath and on the influence of the amplitude of the perturbation on the liquid bridge response.

A. Measurement of surface tension

Since the value of the surface tension, σ , appears in two of the dimensionless parameters [$B = (\rho_i - \rho_o)gR_o^2/\sigma$, $C = \nu(\rho_i/\sigma R_o)^{1/2}$, where ρ_i and ρ_o are the densities of the liquid column and the surrounding liquid, respectively], the knowledge of the value σ during experiments is of paramount importance. The value of σ for silicone oils and methanol-water mixtures has been measured by Bisch, Lasek, and Rodot,⁷⁰ and, according to these authors, the corresponding value for the silicone oil used would be $\sigma = 0.0135 \text{ N m}^{-1}$. In our case the value of σ has been determined by comparing the experimental frequencies of resonance corresponding to the first oscillation mode of cylindrical volume liquid bridges with those predicted by the three-dimensional model (which includes bath effects) developed by Sanz.^{29,71} Since such a model only applies to liquid bridges in gravitationless conditions, these previous experiments were performed using short liquid bridges in order to minimize gravity effects. Other experimental conditions were equal disks ($K = 1$) and cylindrical volume. Experimental results are shown in Table I. In this table the values of the slenderness, Λ , and frequency of resonance, f , are those measured during the experiments, whereas ω_b corresponds to the theoretical values calculated by Sanz⁷¹ for liquid bridges of the same slenderness placed in an outer medium of the same density ($\rho_i = \rho_o$); note that in the theoretical case $B = 0$, so that these experiments have been performed with low slenderness liquid bridges, because in such configurations gravity effects are negligible, provided the value of ρ_o is close enough to that of ρ_i .

The values of σ in Table I have been calculated by taking into account that the dimensionless pulsation, ω , is related to the frequency, f , through

$$\omega_b = 2\pi f(\rho_i R_o^3/\sigma)^{1/2}. \quad (78)$$

According to the values of σ included in Table I, the average value $\sigma = 0.0125 \text{ N m}^{-1}$ has been taken for our

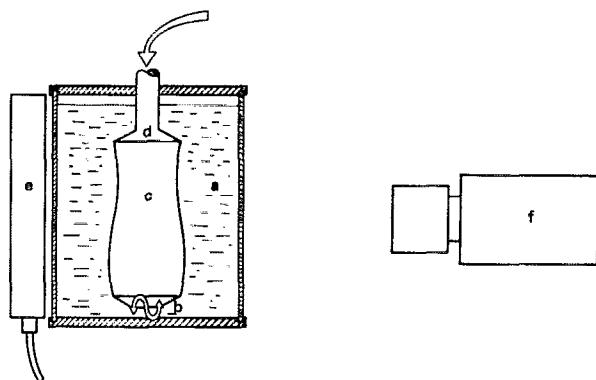


FIG. 17. Experimental arrangement: (a) Plateau tank; (b) oscillating disk; (c) liquid bridge; (d) injection duct; (e) illumination; and (f) CCD camera.

TABLE I. Results of the experiments for the measurement of the value of surface tension, σ .

Λ	f (Hz)	ω_b^a	σ (N m ⁻¹)
1.30	0.518	1.664	0.0121
1.37	0.474	1.500	0.0125
1.47	0.418	1.296	0.0130
1.48	0.401	1.273	0.0124
1.67	0.311	0.968	0.0129

^a The values of ω_b in the table have been obtained from Fig. 5.5 of Sanz (Ref. 71) and correspond to the case of a liquid bridge inside a bath of the same density, when the walls of the Plateau tank are very far from the liquid bridge axis.

experiments. This value is slightly smaller, some 7%, than the one reported by Bisch *et al.*⁷⁰

B. Influence of the amplitude of the disk oscillation on the response of the liquid bridge

A preliminary set of experiments has been carried out, aiming to establish the relationship between the liquid bridge response and the amplitude of the perturbation. In these experiments the lower disk was sinusoidally oscillated according to the law $(a/2) \sin 2\pi f t$ and the amplitude of the deformation of the liquid bridge interface at $z = \Lambda/2$ was measured. The working configuration was a liquid bridge of slenderness $\Lambda = 2.35$, dimensionless volume $V = 14.8$, and Bond number ranging from 0.028 (at the beginning of the tests) to 0.004 (end of the tests). The results obtained are plotted in Fig. 18, where the vertical size of the different rectangles gives an estimation of the error in experimental values. The results corresponding to $a = 0.46$ mm and $a = 1.24$ mm are almost the same, which seems to indicate that in this range of values of a the liquid bridge response is linear. However, the experimental errors are much larger in the case $a = 0.46$ mm than in $a = 1.24$ mm, the reason being that for the same accuracy in measurements the relative error grows as the value of the measured magnitude decreases.

Concerning the tests made with $a = 2.44$ mm (the errors in this case are similar to those obtained with $a = 1.22$ mm) the most significant characteristic is that in this case results lie under the results obtained with smaller values of a . This can be explained because of nonlinear effects appearing when the perturbation amplitude is large enough. To analyze this nonlinear effect a self-similar one-dimensional Cosserat model for the liquid bridge dynamics (Rivas and Meseguer⁴⁶ and Meseguer *et al.*¹⁸) can be used. This nonlinear

model is only valid for almost cylindrical long liquid bridges ($V \sim 2\pi\Lambda$, $\Lambda \sim \pi$) in an axial microgravity field ($B \sim 0$). Under such circumstances Rivas and Meseguer⁴⁶ demonstrated that the equation that describes the liquid bridge interface evolution is the well-known Duffing equation,

$$\delta_{tt} + C\delta_t + \frac{8}{25}\lambda\delta - \frac{3}{30}\delta^3 + \frac{16}{25}B = 0, \quad (79)$$

where δ is the amplitude of the interface deformation, which is assumed to be of the form $S(z,t) = 1 + \delta(t) \sin \pi z/\Lambda$, λ is a reduced slenderness in which volume effects are included,

$$\lambda = 1 - \frac{\Lambda}{\pi} + \frac{1}{2} \left(\frac{V}{2\pi\Lambda} - 1 \right), \quad (80)$$

and t , B , and C are the dimensionless time, Bond number, and parameter of viscosity, respectively, already defined. Equation (79) admits a self-similar solution that allows the removal of the parameter λ from the formulation. However, in the following λ is retained in order to clearly maintain the physical meaning of the different symbols.

Let us assume that Bond number varies sinusoidally with time and that such time variation is obtained by moving both supporting disks instead of varying the value of g (both effects are similar, as demonstrated in Sec. III). In such a case, if $\alpha = a/2R_0$ is the dimensionless amplitude of the oscillation of the disks and ω the dimensionless pulsation, the acceleration of the liquid bridge would be $(a\omega^2 R_0/t_c^2) \sin \omega t$, where t_c is the characteristic time, $t_c = (\rho_l R_0^3/\sigma)^{1/2}$, and the Bond number

$$B = \frac{\rho_l R_0^2}{\sigma} \frac{R_0}{t_c^2} \alpha \omega^2 \sin \omega t = \alpha \omega^2 \sin \omega t. \quad (81)$$

Therefore Eq. (79) may be written as

$$\delta_{tt} + C\delta_t + \frac{8}{25}\lambda\delta - \frac{3}{30}\delta^3 + \frac{16}{25}\alpha\omega^2 \sin \omega t = 0. \quad (82)$$

For the purposes of this explanation, it will be enough to solve approximately Eq. (82) by using some of the standard methods one can find in the literature.⁷² For instance, assuming the solution can be written as

$$\delta(t) = \sum \delta_{2p+1} \sin(2p+1)\omega t, \quad (83)$$

and introducing the phase shift φ in the forcing term, $B = \alpha\omega^2 \sin(\omega t + \varphi)$, the expression that relates δ_1 with the perturbation (Stoker⁷²) becomes

$$\left[\left(\frac{8}{25}\lambda - \omega^2 \right) \delta_1 - \frac{9}{200} \delta_1^3 \right]^2 + C^2 \omega^2 \delta_1^2 = \frac{256}{225} \alpha^2 \omega^4. \quad (84)$$

The response of the liquid bridge, defined as the ratio of the interface deformation to the perturbation amplitude, $\delta_1/2\alpha$, has been plotted in Fig. 19. These results have been obtained by taking $C = 0.022$ and $\lambda = 0.25$, which are the values corresponding to the experimental configuration ($\Lambda = 2.35$, $V \sim 2\pi\Lambda$). According to this simplified model, the peak of the liquid bridge response decreases as α increases, which coincides with the experimental behavior shown in Fig. 18. Note that analytical results obtained through this simplified model are only qualitative because the model is only applicable when $\Lambda \sim \pi$, far from the value of $\Lambda = 2.35$ used in experiments.

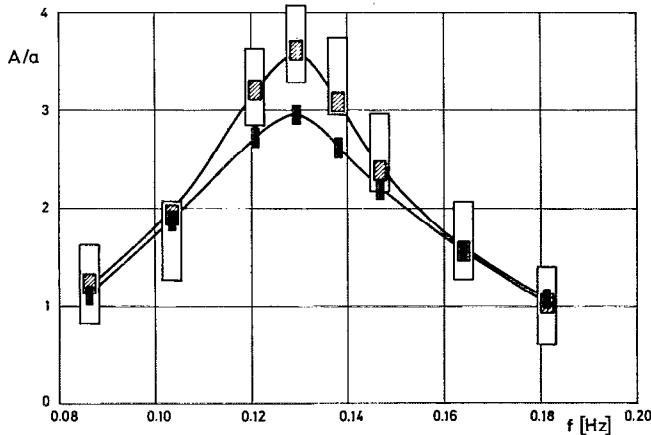


FIG. 18. Variation with the frequency of the disk vibration, f , of the ratio of the amplitude of the interface deformation (measured at $z = \Lambda/2$) to the amplitude of the disk oscillation, A/a . The height of the rectangles indicates the error in A/a . The error in f is the same in all cases, although the rectangles have been plotted with different width to improve data presentation. The type of rectangle indicates the value of a , according to the following key: white, 0.46 mm; striped, 1.24 mm; and black, 2.44 mm.

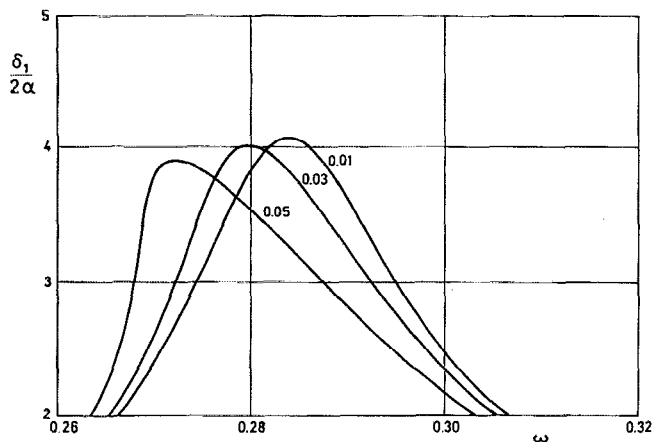


FIG. 19. Variation with the pulsation, ω , of the ratio of the interface deformation to the perturbation amplitude, $\delta_1/2\alpha$, as given by expression (84). Numbers on the curves indicate the value of α .

Finally, according to Fig. 18, it seems that the appropriated value for the amplitude of the disk oscillation is $a = 1.24$ mm, for which the liquid bridge response is still linear, or almost linear, and errors in measurements are acceptable.

C. Dynamic response of long liquid bridges

To compare with theoretical results obtained from the liquid bridge model already presented in Secs. II–IV, several experiments have been performed. In these experiments one of the supporting disks (the lower one) is harmonically oscillated, whereas the opposite disk remains at rest.

The experimental procedure was as follows: once a liquid bridge of the desired volume and slenderness is established its interface shape is determined and stored, as explained in Appendix B. Such an interface shape will be used later to accurately determine the volume of the liquid bridge (by integration of the interface shape along the z axis), as well as the value of the Bond number at the beginning and at the end of the experiments. Bond number is calculated by fitting theoretical equilibrium interface shapes of known volume, V , slenderness, Λ , and disks ratio, K , varying Bond number, B , to experimental interface shapes, trying to minimize the quadratic distance between them (Fig. 20). The same procedure is repeated once an experimental sequence is finished, to obtain a measurement of the variation of the Bond number during such a sequence.

The dynamic response of the liquid bridge is obtained in real time as follows: since the image analysis system allows visualization in a computer screen of the variation with time of the liquid bridge diameter at some prefixed sections, as well as that of the axial displacement of the oscillating disk, once a selected frequency is set, and waiting some four or five cycles in order to reach steady conditions, the amplitude of the liquid bridge oscillation at the selected sections and the phase shift between the liquid bridge response (at selected sections) and disk oscillation are directly obtained by com-

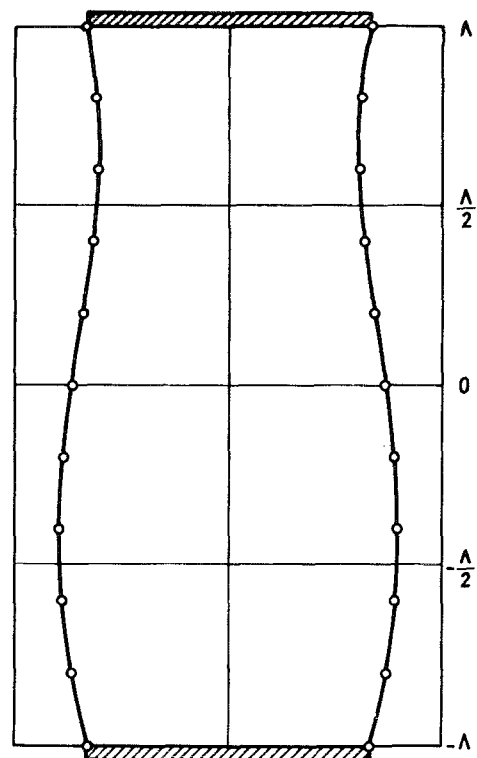


FIG. 20. Liquid bridge with $\lambda = 2.52$, $V = 18.1$, $K = 1$, and $B = -0.056$. The circles indicate the best theoretical fitting to the measured interface shape (continuous line). The horizontal lines correspond to the sections where the variation of radius with time has been measured during experiments.

paring the two appropriated signals. In our case the selected sections were placed at $z = -\Lambda/2$, $z = 0$, and $z = \Lambda/2$; the vibrating disk was the one placed at $z = -\Lambda$, whereas the opposite disk, at $z = \Lambda$, was kept at rest. Once the values of amplitudes and phase shifts are stored a new value of the frequency is set and the above process repeated again.

The main characteristics of the two first runs performed are shown in Table II. Note that taking into account the values of the physical properties of the fluid configuration used ($\rho_l = 936 \text{ kg m}^{-3}$, $\nu = 10^{-5} \text{ m}^2 \text{ sec}^{-1}$, $\sigma = 0.0125 \text{ N m}^{-1}$, $R_0 = 0.015 \text{ m}$), the value of the characteristic time results $t_c = 0.503 \text{ sec}$ and the viscosity parameter is $C = 0.022$. In all the experiments described in this section the peak amplitude of the disk oscillation was 1.24 mm.

TABLE II. Characteristics of the liquid bridge configurations used in experiments (a liquid column of silicone oil DMS-10 placed inside a mixture of methanol and water).

	Run I	Run II
Slenderness, Λ	2.52	2.30
Dimensionless volume, V	18.1 ± 0.2	20.3 ± 0.2
Bond number, B		
at the beginning of the run	-0.056 ± 0.001	-0.139 ± 0.001
at the end of the run	-0.008 ± 0.001	-0.100 ± 0.001
Duration of the run (min)	140	100

To compare experimental and analytical results it should be taken into account that Bond number varies with time within an experimental sequence. This time variation of B is due to alcohol evaporation, so that the density of the methanol–water mixture, ρ_0 , increases with time. As can be observed in Table II, the absolute value of B decreases with time in both experiments. This means that, since both disks are equal in diameter, $K = 1$, in both cases the liquid bridge configuration is more stable at the end of each one of the runs than at the beginning or, in other words, that the frequencies of resonance would be higher at the end of the experimental sequence than at the beginning (Meseguer⁴¹).

This dependence of the frequencies of resonance on the Bond number can be estimated by using the mathematical model presented in Sec. IV. For instance, in the run I case this model predicts for the dimensionless pulsation of resonance, ω , corresponding to the first oscillation mode the value $\omega = 0.38$ when $B = -0.056$ and $\omega = 0.42$ when $B = -0.008$; in a similar fashion, the corresponding values for the run II case are $\omega = 0.55$ ($B = -0.139$) and $\omega = 0.59$ ($B = -0.100$). According to these results the

maximum difference in the values of ω , due to the variation of Bond number along the sequence, is of the order of 10%.

Therefore the liquid bridge response could be theoretically calculated, assuming the Bond number varies with time, but this would introduce a new parameter, to be taken into account when comparing theoretical and experimental results. In the following experimental results are compared with theoretical ones calculated under the assumption that Bond number does not change with time, the reference value of B used in calculations being that measured at the beginning of the experimental sequences. This comparison is shown in Fig. 21. In this plot the ratio of the peak amplitude of the interface oscillation at selected sections to the radius of the disks, A/R_0 , has been represented as a function of the dimensionless pulsation, ω , of the oscillating disk. As can be observed, experimental data show the same trends as theoretical results, although experiments give lower values of the frequencies of resonance than the Cosserat model, the differences increasing as the oscillation mode increases. These differences can be explained because of two reasons, at least. The first reason concerns nonlinear effects that become more

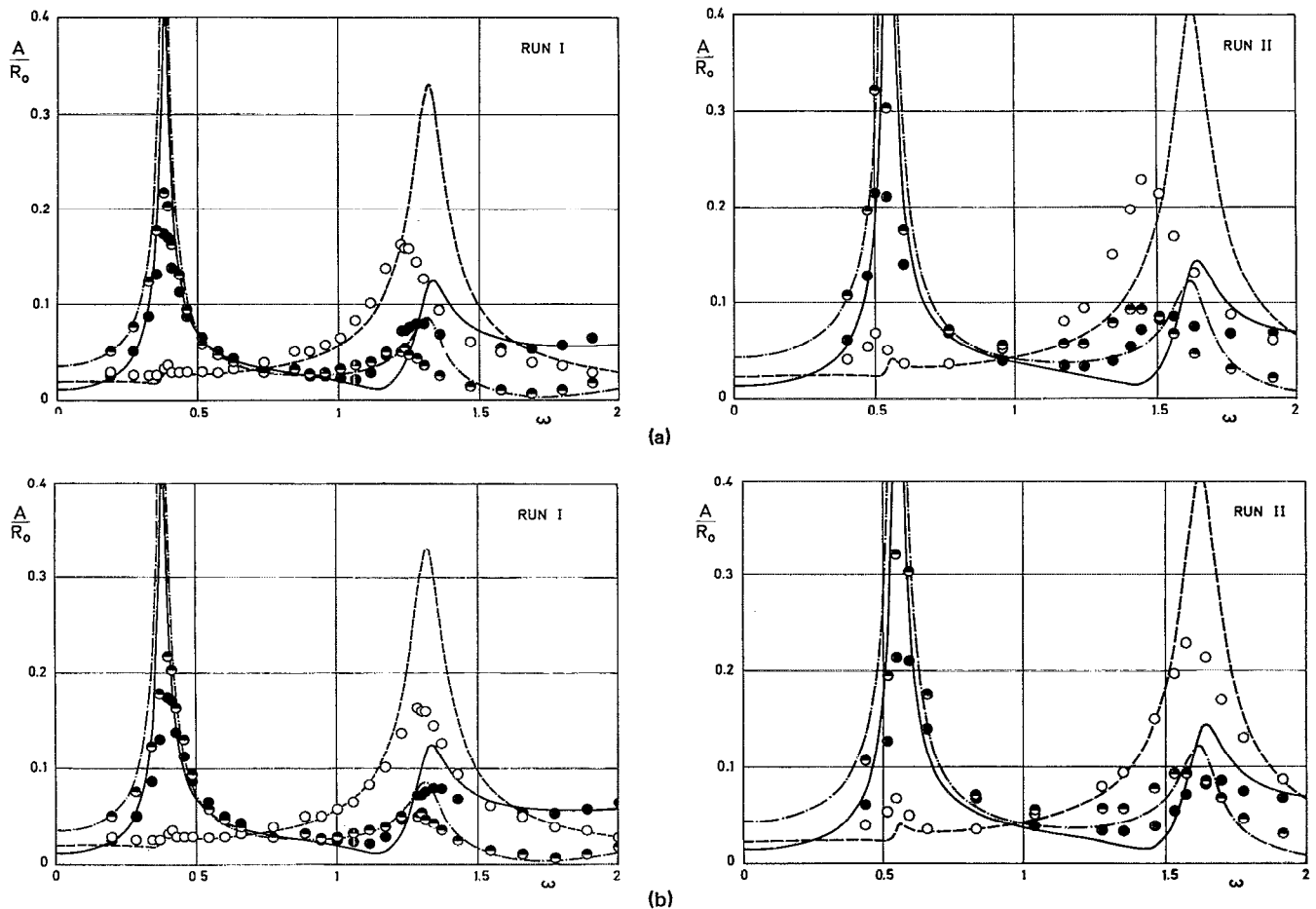


FIG. 21. Variation with the pulsation, ω , of the amplitude of the oscillation of the liquid bridge interface at selected sections. Liquid bridge configurations are defined in Table II. Line type (symbol) indicates theoretical (experimental) results according to the following key: - - (○) obtained at section $\Lambda/2$; - - - (○) obtained at section 0; and — (●) obtained at section $\Lambda/2$. Experimental results in (a) have not been corrected to take into account outer bath effects. The same experimental results multiplied by the appropriated factor to take into account bath effects (0.95 for $\Lambda = 2.52$ and 0.92 for $\Lambda = 2.30$) are shown in (b).

and more important as ω grows. The second reason deals with the effect of the outer bath in the frequencies of resonance. In effect, experimental results in Fig. 21(a) have been obtained by using the neutral buoyancy technique, whereas in the mathematical model the effect of an outer liquid of the same density of the liquid bridge has not been considered.

The effect of the outer bath on the dynamics of liquid bridges was analyzed by Sanz^{29,71} in the case $V = 2\pi\Lambda$, $B = 0$, $K = 1$. According to this author the frequencies are smaller as the density, ρ_0 , of the surrounding bath increases, in such a way that when $\rho_0 \sim \rho_l$, provided the walls of the Plateau tank are far enough, the calculated frequency of resonance corresponding to the first mode is a fraction of the value calculated when $\rho_0 \ll \rho_l$, this fraction being 0.82 at $\Lambda = 1$ and 0.91 at $\Lambda = 2.9$. Unfortunately, the results obtained by Sanz^{29,71} only apply to cylindrical liquid bridges in gravitationless conditions, which are far from the fluid configurations used in our experiments. However, one could expect a similar behavior in the case $V \neq 2\pi\Lambda$ and $B \neq 0$. For instance, experimental and theoretical results are compared again in Fig. 21(b), but in this case experimental results have been divided by appropriated factors to take into account bath effects. The factors used have been 0.95 (run I, $\Lambda = 2.52$) and 0.92 (run II, $\Lambda = 2.30$), close enough to the values calculated by Sanz^{29,71} for cylindrical volume liquid bridges.

In any case, it should be pointed out that the mathematical model accurately predicts the experimental behavior, except in the resonances, in which the measured values of A/R_0 are much smaller than the predicted ones. This difference can be also explained if it is taken into account the effect of the surrounding bath, which introduces a damping on the liquid bridge dynamics, this damping effect being higher as the deformation of the liquid bridge interface increases.

In Fig. 22 the phase shift, φ , between the oscillation of the forcing disk and that of the liquid bridge at section $z = -\Lambda/2$ has been represented. Experimental results cor-

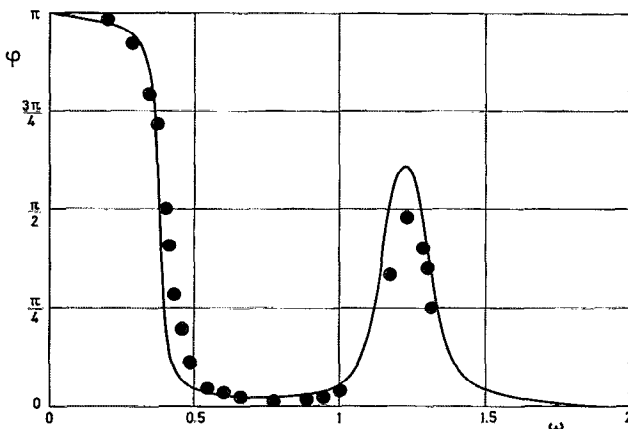


FIG. 22. Phase shift, φ , between the interface oscillation at section $z = -\Lambda/2$ and the disk oscillation. Results corresponding to Run I (see Table II). The line indicates theoretical results, whereas the symbols indicate corrected experimental ones.

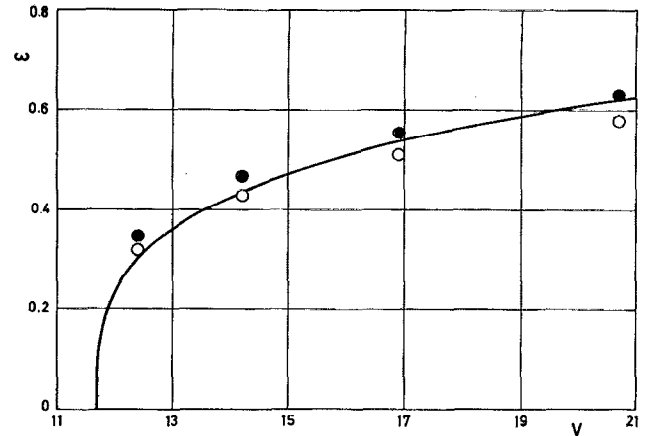


FIG. 23. Variation with the volume, V , of the first pulsation of resonance, ω , of liquid bridges with $\Lambda = 2.30$, $K = 1$, $C = 0.022$, and $B \approx -0.07$. The line corresponds to theoretical results, whereas the symbols indicate uncorrected experimental results (white circles) or corrected experimental results, to take into account the effect of the outer bath (black circles).

respond to run I, and in this case a correction factor for the frequencies equal to 0.95 has also been used. Also, in this case there is a very good agreement between theoretical and experimental results, which gives an idea of the accuracy of this Cosserat model in predicting the dynamics of axisymmetric liquid bridges. The phenomenon of the double crossing by $\varphi = \pi/2$ already mentioned in Sec. III can also be observed.

The influence of the volume on the first frequency of resonance is shown in Fig. 23. In these additional experiments a liquid bridge with $\Lambda = 2.30$ was tested, the average value of Bond number during the experimental sequence being $B = -0.07$. In Fig. 23 the white circles indicate experimental results as measured, whereas the black circles are the same experimental values divided by 0.92 to take into account the effect of the surrounding bath.

Finally, in Table III, the frequencies of resonance measured aboard Spacelab-D1 (Meseguer⁴¹) are compared with the ones predicted by the Cosserat model for the same experimental configurations, and those calculated by Zhang and Alexander,⁴⁵ by using a nonlinear slice model, which includes viscosity effects for the dynamics of cylindrical-volume liquid bridges. The nonlinear results lie between the

TABLE III. Dimensionless pulsation corresponding to the first resonance of liquid bridges between equal disks ($K = 1$) of slenderness Λ and dimensionless volume V in a microgravity field, whose average value is measured by the Bond number B . The subscripts e , c , and z indicate experimental values (Spacelab-D1) and theoretical values obtained by using the linearized Cosserat model or the nonlinear slice model derived by Zhang and Alexander (Ref. 45), respectively.

Λ	$V \pm 0.05$	B	$\omega_e \pm 0.01$	ω_c	ω_z
2.571	16.28	0.009	0.30	0.338	0.312
2.714	16.82	0.009	0.23	0.252	0.248
2.854	18.84	0.009	0.19	0.216	0.174
2.857	17.92	0.010	0.14	0.171	...

linearized Cosserat results and the experimentally obtained values. Experiments aboard Spacelab-D1 were carried out by using silicone oil with the following nominal physical characteristics: $\rho_i = 920 \text{ kg m}^{-3}$, $\nu = 5 \times 10^{-6} \text{ m}^2 \text{ sec}^{-1}$ and $\sigma = 0.02 \text{ N m}^{-1}$. Both disks were equal in diameter ($K = 1$) with $R_0 = 0.0175 \text{ m}$. Theoretical results are some 10% higher than experimental ones, and this difference is probably due to the value of σ used to make dimensionless experimental results. Note that if a variation of 20% in the nominal value of σ is accepted, theoretical and experimental results are practically in agreement.

ACKNOWLEDGMENTS

We wish to thank Dr. Sanz for his helpful discussions.

This work has been supported by the Spanish Comisión Interministerial de Ciencia y Tecnología (Project No. ESP 88-0359).

APPENDIX A: COSSERAT MODEL GENERATION

The problem of the isothermal, axisymmetric liquid bridge dynamics is governed by the following nondimensional formulation:

continuity equation,

$$(1/r)(rU)_r + W_z = 0; \quad (\text{A1})$$

radial momentum conservation,

$$U_t + UU_r + WU_z = -P_r + C \left(U_{zz} + U_{rr} + \frac{1}{r} U_r - \frac{1}{r^2} U \right); \quad (\text{A2})$$

axial momentum conservation,

$$W_t + UW_r + WW_z = -P_z + C \left(W_{zz} + W_{rr} + \frac{1}{r} W_r \right); \quad (\text{A3})$$

boundary conditions at the bridge axis,

$$U(z, 0, t) = 0, \quad W_r(z, 0, t) = 0; \quad (\text{A4})$$

normal stress equilibrium of the interface [$r = F(z, t)$],

$$P - \frac{2C}{1 + (F_z)^2} [U_r + (F_z)^2 W_z - F_z (W_r + U_z)] = P_c, \quad (\text{A5})$$

where P_c accounts for the capillary pressure jump across the interface;

tangential stress equilibrium of the interface,

$$C \{ 2F_z (U_r - W_z) + [1 - (F_z)^2] (W_r + U_z) \} = 0; \quad (\text{A6})$$

and kinematic boundary condition,

$$F_t - U + WF_z = 0. \quad (\text{A7})$$

This formulation must be completed with suitable boundary conditions for the axial and radial velocity at the disks and the condition of the anchoring of the interface to the edges of the disks, situated in a position given, in first approximation, by $z = \pm \Lambda$.

Since the problem under consideration concerns the dy-

namics of long liquid bridges ($\Lambda \gg 1$), let us introduce as a small parameter of the problem $\epsilon = R/L = 1/2\Lambda \ll 1$ and rescale all the variables involved by setting

$$r = r, \quad y = \epsilon z, \quad t = t, \quad W = W, \quad V = \epsilon^{-1} U, \quad (\text{A8})$$

where the last scaling is suggested by Eq. (A1).

With the new variables the formulation now reads

$$(1/r)(rV)_r + W_y = 0, \quad (\text{A9})$$

$$V_t + \epsilon VV_r + \epsilon WW_y = -\frac{1}{\epsilon} P_r + C \left(\epsilon^2 V_{yy} + V_{rr} + \frac{1}{r} V_r - \frac{1}{r^2} V \right), \quad (\text{A10})$$

$$W_t + \epsilon VW_r + \epsilon WW_y = -\epsilon P_y + C \left(\epsilon^2 W_{yy} + W_{rr} + \frac{1}{r} W_r \right), \quad (\text{A11})$$

plus the new boundary and initial conditions. Now both the radial coordinate r and the axial coordinate y are of order unity.

In the inviscid case it can be deduced that the radial variations of the axial velocity are negligible when compared with W (Meseguer³⁸),

$$\Delta_{\text{radial}} W \sim \epsilon^2 \Delta_{\text{axial}} W, \quad (\text{A12})$$

and for the viscous case a similar relationship can be obtained from boundary condition (A6).

From Eq. (A10) it can be deduced that $P_r/\epsilon \sim V_t \sim 1$, and consequently $P_r \sim \epsilon$. On the other hand, from Eq. (A11) $\epsilon P_y \sim W_t \sim 1$, so that P could be expanded as $P = P_0/\epsilon + \epsilon P_1 + \dots$; however, this is in contradiction with boundary condition (A5), which states that $P \sim 1$. From this order of magnitude analysis it follows that the characteristic time of the phenomenon is not of order unity, as initially can be thought, but of order ϵ^{-1} (which is in agreement with the evolution times observed in capillary evolutions). If a rescaled time (of order unity) is introduced, $\tau = \epsilon t$, Eqs. (A10) and (A11) become

$$V_\tau + VV_r + WW_y = -\frac{1}{\epsilon^2} P_r + \frac{C}{\epsilon} \left(\epsilon^2 V_{yy} + V_{rr} + \frac{1}{r} V_r - \frac{1}{r^2} V \right), \quad (\text{A13})$$

$$W_\tau + VW_r + WW_y = -P_y + \frac{C}{\epsilon} \left(\epsilon^2 W_{yy} + W_{rr} + \frac{1}{r} W_r \right). \quad (\text{A14})$$

In view of (A13) and (A14), V , W , and P can be expanded as

$$V = V_0(y, r, \tau) + \epsilon^2 V_2(y, r, \tau) + \dots, \quad (\text{A15})$$

$$W = W_0(y, r, \tau) + \epsilon^2 W_2(y, r, \tau) + \dots, \quad (\text{A16})$$

$$P = P_0(y, r, \tau) + \epsilon^2 P_2(y, r, \tau) + \dots, \quad (\text{A17})$$

so that Eq. (A14) gives

$$W_{0,\tau} + V_0 W_{0,r} + W_0 W_{0,y} + \epsilon^2 (W_{2,\tau} + V_0 W_{2,r} + V_2 W_{0,r} + W_0 W_{2,y} + W_2 W_{0,y}) + \dots$$

$$= -P_{0y} - \epsilon^2 P_{2y} + \frac{C}{\epsilon} \left(W_{0r} + \frac{1}{r} W_{0r} \right) + C \epsilon \left(W_{0yy} + W_{2rr} + \frac{1}{r} W_{2r} \right) + \dots \quad (\text{A18})$$

Note that if $C \sim 1$ the ϵ^{-1} problem would give $W_{0r} + (1/r) W_{0r} = 0$, that is, $W_0 = W_0(y, t)$, which, together with the above reasoning on the radial variation of W , seems to indicate that W_0 can be considered independent of r , not only for small viscosities and, consequently, it can be written as

$$W = W_0(y, t) + \epsilon^2 W_2(y, r, t) + \dots \quad (\text{A19})$$

For the radial velocity, V , taking into account the continuity equation, the expansion would be of the form

$$V = -\frac{1}{2} r W_{0y}(y, t) + \epsilon^2 V_2(y, r, t) + \dots \quad (\text{A20})$$

On the other hand, the ϵ^{-2} problem in Eq. (A13) gives $P_{0r} = 0$, so that

$$P = P_0(y, t) + \epsilon^2 P_2(y, r, t) + \dots \quad (\text{A21})$$

The introduction of expansions (A19), (A20), and (A21) in Eqs. (A8), (A13), and (A14) gives the following: Continuity equation:

$$(1/r)(rV_j)_r + W_j = 0, \quad j = 2, 4, \dots \quad (\text{A22})$$

Note that the continuity equation is fulfilled automatically at order unity [it was taken into account when expansion (A20) was postulated].

Radial momentum equation:

Order 1,

$$-\frac{1}{2} r W_{0yy} + \frac{1}{4} r (W_{0y})^2 - \frac{1}{2} r W_0 W_{0yy} = -P_{2r}; \quad (\text{A23})$$

order ϵ^2 ,

$$V_{2r} - \frac{1}{2} r W_{0y} V_{2r} - \frac{1}{2} W_{0y} V_2 - \frac{1}{2} r W_{0yy} W_2 + W_0 V_{2y} = -P_{4r} + \frac{C}{\epsilon} \left(-\frac{1}{2} r W_{0yyy} + V_{2rr} + \frac{1}{r} V_{2r} - \frac{1}{r^2} V_2 \right). \quad (\text{A24})$$

Axial momentum equation:

Order 1,

$$W_{0r} + W_0 W_{0y} = -P_{0y}; \quad (\text{A25})$$

order ϵ^2 ,

$$W_{2r} - \frac{1}{2} r W_{0y} W_{2r} + W_0 W_{2y} + W_{0y} W_2 = -P_{2y} + \frac{C}{\epsilon} \left(W_{0yy} + W_{2rr} + \frac{1}{r} W_{2r} \right), \quad (\text{A26})$$

where it has been assumed that $C \sim \epsilon$. This formulation must be completed with the appropriate boundary and initial conditions.

In order to generate the so-called Cosserat model two steps shall be followed: first, in the order unity problem some terms that are of ϵ^2 order will be retained [this is not inconsistent if only the $O(1)$ problem is solved]; and second, pressure terms will be eliminated from the formulation by using

boundary conditions at the interface. The resulting $O(1)$ problem is (in the following the subscript "0" has been omitted and the primitive variables have been recovered):

$$-\frac{1}{2} r \left((W_t + WW_z)_z - \frac{3}{2} (W_z)^2 \right) = -P_r - \frac{1}{2} r C W_{zzz}, \quad (\text{A27})$$

$$W_t + WW_z = -P_z + C W_{zz}, \quad (\text{A28})$$

where the underlined terms are of ϵ^2 order and an additional ϵ^2 term in P_z has been considered.

Boundary conditions at the interface now read

$$P(F) - 2C [1 + (F_z)^2]^{-1} [W_z(2(F_z)^2 - 1) + FF_z W_{zz}] = P_c, \quad (\text{A29})$$

$$6F_z W_z = F [(F_z)^2 - 1] W_{zz}, \quad (\text{A30})$$

$$2F_t + FW_z + 2F_z W = 0, \quad (\text{A31})$$

where Eq. (A31) can be reduced to the continuity equation of a slice $(F^2)_t + (F^2 W)_z = 0$.

Equation (A27) states that P_r must be linear in r (and of order ϵ^2), so that momentum equations (A27) and (A28) suggest that pressure is of the form

$$P(r, z, t) = \frac{1}{2} r^2 A(z, t) + h(z, t), \quad (\text{A32})$$

where $h(z, t) \sim 1$ and $A(z, t) \sim \epsilon^2 \ll h(z, t)$. Introduction of this expression for P in (A27) and (A28) gives

$$(W_t + WW_z)_z - \frac{3}{2} (W_z)^2 = 2A + C W_{zzz}, \quad (\text{A33})$$

$$W_t + WW_z = -\frac{1}{2} r^2 A_z - h_z + C W_{zz}. \quad (\text{A34})$$

Observe that in Eq. (A34) all terms of order unity depend only on z and t , but there is an additional retained term of order ϵ^2 , which depends on r, z , and t . To eliminate r from the formulation, Eq. (A34) is substituted by its integral over a slice, that is,

$$F^2 (W_t + WW_z) = -\frac{1}{2} F^4 A_z - F^2 h_z + C F^2 W_{zz}. \quad (\text{A35})$$

Note that there are three unknowns: $F(z, t)$, $W(z, t)$, and $P(r, z, t)$ [that is, $A(z, t)$ and $h(z, t)$], and three equations: continuity equation and two momentum equations, (A33) and (A34). There are four boundary conditions at the disks (two at each one of the disks) and two more equations at the interface, (A29) and (A30). The formulation must be completed, of course, with suitable initial conditions.

To eliminate pressure terms from the formulation, boundary conditions at the interface are rewritten as the equilibrium of the stresses in axial direction and in radial direction, instead of in the normal direction, Eq. (A29), and in the tangential direction, Eq. (A30). These conditions are, in the radial direction,

$$\frac{1}{2} F^2 A + h = C (-W_z + \frac{1}{2} FF_z W_{zz}) + P_c, \quad (\text{A36})$$

and in the axial direction,

$$\frac{1}{2} F^2 A + h = C \left(2W_z + \frac{1}{2} \frac{F}{F_z} W_{zz} \right) + P_c. \quad (\text{A37})$$

Let us multiply Eq. (A33) by $F^4/8$ and introduce the function $\mathcal{P} = \frac{1}{4} F^4 A + F^2 h$ (proportional to the integral of

the pressure in each slice). Then, the second member of (A38), taking into account the definition of \mathcal{P} and (A36), becomes

$$\begin{aligned} \frac{1}{4}F^4A + \frac{1}{8}CF^4W_{zz} \\ = F^2(\frac{1}{2}F^2A + h) - P + \frac{1}{8}CF^4W_{zz} \\ = -\mathcal{P} + \frac{1}{8}C[(F^4W_{zz})_z - 8F^2W_z] \\ + F^2P_c, \end{aligned} \quad (\text{A38})$$

and the second term of (A35), with the help of (A37), can be written as

$$\begin{aligned} -\frac{1}{4}F^4A_z - F^2h_z + CF^2W_{zz} \\ = -\mathcal{P}_z + 2FF_z(\frac{1}{2}F^2A + h) + CF^2W_{zz} \\ = -\mathcal{P}_z + 2C(F^2W_z)_z + (F^2)_zP_c; \end{aligned} \quad (\text{A39})$$

therefore the momentum equations become

$$F^2(W_t + WW_z) = -\mathcal{P}_z + (F^2)_zP_c + 2C(F^2W_z)_z, \quad (\text{A40})$$

$$\begin{aligned} \frac{1}{8}F^4[(W_t + WW_z)_z - \frac{1}{2}(W_z)^2] \\ = -\mathcal{P} + F^2P_c + \frac{1}{8}C[(F^4W_{zz})_z - 8F^2W_z], \end{aligned} \quad (\text{A41})$$

which are identical to those known as Cosserat equations.

APPENDIX B: INTERFACE SHAPE ANALYSIS

The measurements of both the interface equilibrium shape and the deformation versus time of given sections when the liquid bridge is excited have been made by analyzing

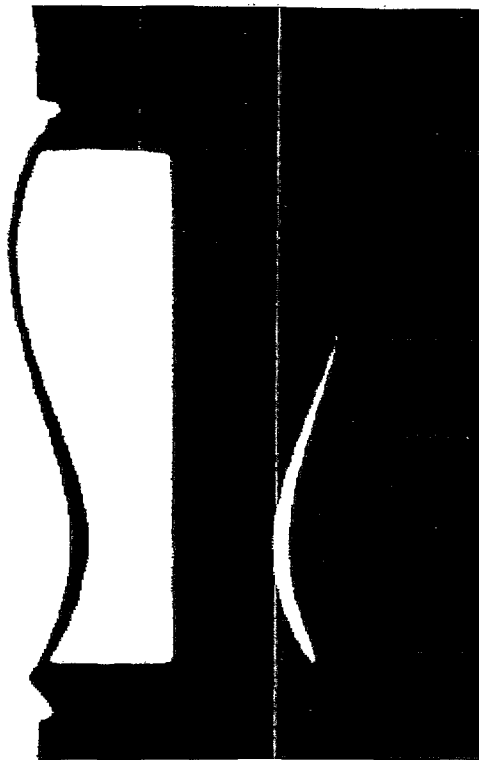


FIG. 24. Typical image of a liquid bridge illuminated, as described in Appendix B.

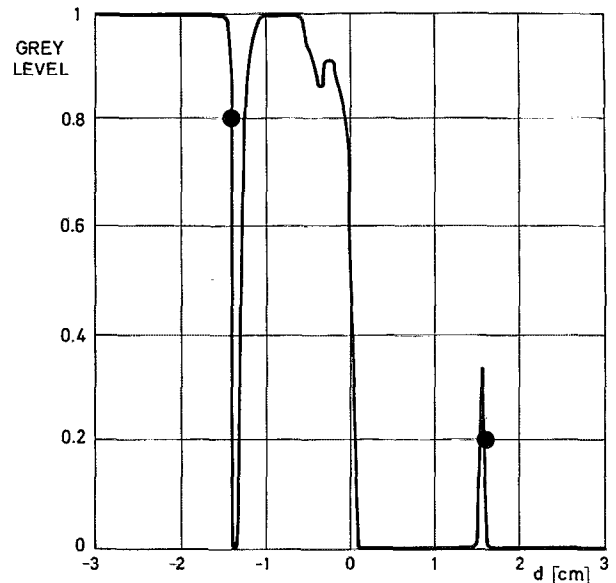


FIG. 25. Distribution of grey level along a horizontal line of the picture shown in Fig. 24. In this plot d indicates the distance from the liquid bridge axis.

ing the video image obtained by a CCD camera. It is of the utmost importance to choose the illumination system suited to the desired application. In these experiments, due to the difference in refractive index between the outer bath (water-methanol mixture) and the fluid of the liquid bridge (silicone oil), it is easy to obtain a highly contrasted image by using a uniform background illumination for only half of the field, in such a way that, when seen from the camera side, the border of the illuminated region coincides with the projection of the liquid bridge axis (Fig. 24). A typical brightness profile of a horizontal line of the picture shown in Fig. 24 can be seen in Fig. 25. On the left side ($d < -1.5$ cm), the illuminated background region can be seen through the bath, whereas the right part ($d > 1.5$ cm) corresponds to the nonilluminated region. The liquid bridge borders can be seen as a narrow dark band in the bright side (the left border) and a narrow bright band in the dark one (the right border). These bands correspond to the nonilluminated and illuminated regions of the opposite half background seen through the liquid bridge, which acts as a lens. In this way, the interface shape can be determined by looking at the point where the sharp transition between bright and dark occurs.

The image coming from the CCD camera, once digitized, is scanned line by line (the digitizer has a resolution of 512 lines of 512 pixels each) searching the pixels in which the transition from dark to bright occurs (the interface left border) and from bright to dark (the right one). The interface is assumed to be in the point where the illumination is 80% of the maximum (for the left border) and 20% (for the right one), as indicated in Fig. 25, and these points can be easily computed by linear interpolation between the grey levels of the two adjacent pixels. From this measurement the interface equilibrium shape can be determined (see Fig. 20) and stored in a few seconds. The recording of the liquid bridge

evolution on a VTR has not been used because during analysis after the experiment it is difficult to synchronize consecutive images due to the degradation of the signal. Thus real time analysis has been preferred. Due to the limited computer capabilities, only the evolution with time of the diameter of given sections (three sections in the experiments performed) can be monitored at the video full rate (25 times per second).

- ¹W. R. Wilcox, "Zone refining," *Encycl. Chem. Technol.* **24**, 903 (1984).
- ²A. D. Myshkii, V. G. Babskii, N. D. Kopachevskii, L. A. Slobozhanin, and A. D. Tyupsov, *Low-Gravity Fluid Mechanics* (Springer-Verlag, Berlin, 1987).
- ³J. M. Haynes, "Stability of a fluid cylinder," *J. Colloid Interface Sci.* **32**, 652 (1970).
- ⁴M. A. Erle, R. D. Gillette, and D. C. Dyson, "Stability of interfaces of revolution with constant surface tension. The case of the catenoid," *Chem. Eng. J.* **1**, 97 (1970).
- ⁵R. D. Gillette and R. C. Dyson, "Stability of fluid interfaces of revolution between equal solid circular plates," *Chem. Eng. J.* **2**, 44 (1971).
- ⁶S. R. Coriell and M. R. Cordes, "Theory of molten zone shape and stability," *J. Cryst. Growth* **42**, 466 (1977).
- ⁷I. Martínez, "Floating zone. Equilibrium shapes and stability criteria," in *COSPAR Space Research XVIII* (Pergamon, Oxford, 1978), p. 519.
- ⁸E. A. Boucher and M. J. B. Evans, "Capillary phenomena, Part XII. Properties of fluid bridges between solids in a gravitational field," *J. Colloid Interface Sci.* **75**, 409 (1980).
- ⁹L. A. Slobozhanin, "Problems on the stability of liquids in equilibrium, appearing in spatial technology," in *Hydromechanics and Heat and Mass Transfer in Zero-Gravity* (Nauka, Moscow, 1982), Vol. 9 (in Russian).
- ¹⁰M. J. Russo and P. H. Steen, "Instability of rotund capillary bridges to general disturbances, experiment and theory," *J. Colloid Interface Sci.* **113**, 154 (1986).
- ¹¹J. M. Perales, "Non-axisymmetric effects on long liquid bridges," *Acta Astronaut.* **15**, 561 (1987).
- ¹²E. A. Boucher and T. G. Jones, "Equilibrium and stability characteristics of zero-gravity fluid bridges constrained between equal solid rods," *J. Colloid Interface Sci.* **126**, 469 (1988).
- ¹³S. R. Coriell, S. C. Hardy, and M. R. Cordes, "Stability of liquid zones," *J. Colloid Interface Sci.* **60**, 126 (1977).
- ¹⁴I. Da Riva and I. Martínez, "Floating zone stability (Exp. I-ES-331)," in *ESA SP-142* (ESA Publication Division, ESTEC, Noordwijk, 1979), p. 79.
- ¹⁵J. Meseguer, "Stability of long liquid columns," in *ESA SP-222* (ESA Publication Division, ESTEC, Noordwijk, 1984), p. 297.
- ¹⁶J. Meseguer, "Stability of slender, axisymmetric liquid bridges between unequal disks," *J. Cryst. Growth* **67**, 141 (1984).
- ¹⁷I. Martínez and J. M. Perales, "Liquid bridge stability data," *J. Cryst. Growth* **78**, 369 (1986).
- ¹⁸J. Meseguer, A. Sanz, and J. M. Perales, "Axisymmetric long liquid bridges stability and resonances," *Appl. Microgravity Technol.* **2**, 186 (1990).
- ¹⁹I. Martínez, "Floating zone under reduced gravity. Axisymmetric equilibrium shapes," in *ESA SP-114* (ESA Publication Division, ESTEC, Noordwijk, 1976), p. 277.
- ²⁰I. Martínez, "Stability of axisymmetric liquid bridges," in *ESA SP-191* (ESA Publication Division, ESTEC, Noordwijk, 1983), p. 267.
- ²¹R. A. Brown and L. E. Scriven, "The shapes and stability of captive rotating drops," *Philos. Trans. R. Soc. London Ser. A* **297**, 51 (1980).
- ²²I. Da Riva, "Stability of liquid bridges," in *Applications of Space Technology* (Pergamon, Oxford, 1981), p. 69.
- ²³L. H. Ungar and R. A. Brown, "The dependence of the shape and stability of captive rotating drops on multiple parameters," *Philos. Trans. R. Soc. London Ser. A* **306**, 347 (1982).
- ²⁴J. M. Vega and J. M. Perales, "Almost cylindrical isorotating liquid bridges for small Bond numbers," in *ESA SP-191* (ESA Publication Division, ESTEC, Noordwijk, 1983), p. 247.
- ²⁵J. M. Perales, A. Sanz, and D. Rivas, "Eccentric rotation of a liquid bridge," *Appl. Microgravity Technol.* **2**, 193 (1990).
- ²⁶W. Heywang, "Zur Stabilität senkrechter Schmelzzonen," *Z. Naturforsch. teil A* **11**, 238 (1956).
- ²⁷I. Martínez and J. M. Perales, "Bidimensional liquid bridges in a gravity field," *Acta Astronaut.* **15**, 567 (1987).
- ²⁸J. M. Perales, J. Meseguer, and I. Martínez, "Minimum volume of axisymmetric liquid bridges between unequal disks in an axial microgravity field," *J. Cryst. Growth* **110**, 855 (1991).
- ²⁹A. Sanz, "The influence of the outer bath on the dynamics of axisymmetric liquid bridges," *J. Fluid Mech.* **156**, 101 (1985).
- ³⁰H. F. Bauer, "Natural frequencies and stability of immiscible cylindrical z-independent liquid systems," *Appl. Microgravity Technol.* **1**, 11 (1987).
- ³¹H. F. Bauer, "Natural frequencies and stability of circular cylindrical immiscible liquid systems," *Appl. Microgravity Technol.* **2**, 27 (1989).
- ³²A. Gañán, "Análisis modal de zonas líquidas axilísimétricas confinadas por tensión superficial," Tesis doctoral, Universidad de Sevilla, 1989.
- ³³A. Sanz and J. López-Díez, "Non-axisymmetric oscillations of liquid bridges," *J. Fluid Mech.* **205**, 503 (1989).
- ³⁴I. Da Riva and J. Meseguer, "On the structure of the floating zone in melting," *Acta Astronaut.* **5**, 637 (1978).
- ³⁵I. Da Riva and D. R. Manzano, "Impulsive motions of the floating zone," *Physicochem. Hydrodyn.* **2**, 165 (1981).
- ³⁶G. M. Harriot and R. A. Brown, "Flow in a differentially rotated cylindrical drop at low Reynolds number," *J. Fluid Mech.* **126**, 269 (1983).
- ³⁷G. M. Harriot and R. A. Brown, "Flow in a differentially rotated cylindrical drop at moderate Reynolds number," *J. Fluid Mech.* **144**, 403 (1984).
- ³⁸J. Meseguer, "The breaking of axisymmetric slender liquid bridges," *J. Fluid Mech.* **130**, 123 (1983).
- ³⁹J. Meseguer, "The influence of axial microgravity on the breakage of axisymmetric slender liquid bridges," *J. Cryst. Growth* **62**, 577 (1983).
- ⁴⁰J. Meseguer, "The dynamics of axisymmetric slender liquid bridges between unequal discs," *J. Cryst. Growth* **73**, 599 (1985).
- ⁴¹J. Meseguer, "Axisymmetric long liquid bridges in a time-dependent microgravity field," *Appl. Microgravity Technol.* **1**, 136 (1988).
- ⁴²J. Meseguer, A. Sanz, and D. Rivas, "The breaking of axisymmetric non-cylindrical liquid bridges," in *ESA SP-191* (ESA Publication Division, ESTEC, Noordwijk, 1983), p. 261.
- ⁴³J. Meseguer and A. Sanz, "Numerical and experimental study of the dynamics of axisymmetric liquid bridges," *J. Fluid Mech.* **153**, 83 (1985).
- ⁴⁴J. Meseguer and A. Sanz, "One-dimensional linear analysis of the liquid injection or removal in a liquid bridge," *Acta Astronaut.* **15**, 573 (1987).
- ⁴⁵Y. Zhang and J. I. D. Alexander, "Sensitivity of liquid bridges subject to axial residual acceleration," *Phys. Fluids A* **2**, 1966 (1990).
- ⁴⁶D. Rivas and J. Meseguer, "One-dimensional, self-similar solution of the dynamics of axisymmetric slender liquid bridges," *J. Fluid Mech.* **138**, 417 (1984).
- ⁴⁷J. Meseguer and J. M. Perales, "A linear analysis of g-jitter effects on viscous cylindrical liquid bridges," *Phys. Fluids A* **3**, 2332 (1991).
- ⁴⁸G. C. Mason, "An experimental determination of the stable length of cylindrical liquid bubbles," *J. Colloid Interface Sci.* **32**, 172 (1970).
- ⁴⁹A. Sanz and I. Martínez, "Minimum volume for a liquid bridge between equal disks," *J. Colloid Interface Sci.* **93**, 235 (1983).
- ⁵⁰J. Meseguer, L. A. Mayo, J. C. Llorente, and A. Fernández, "Experiments with liquid bridges in simulated microgravity," *J. Cryst. Growth* **73**, 609 (1985).
- ⁵¹J. Meseguer, A. Sanz, and J. López, "Liquid bridge breakages aboard Spacelab-D1," *J. Cryst. Growth* **78**, 325 (1986).
- ⁵²I. Martínez and A. Sanz, "Long liquid bridges aboard sounding rockets," *ESA J.* **9**, 323 (1985).
- ⁵³A. Sanz and J. M. Perales, "Liquid bridge formation," *Appl. Microgravity Technol.* **2**, 133 (1989).
- ⁵⁴J. R. Carruthers and M. Grasso, "Studies of floating liquid zones in simulated zero gravity," *J. Appl. Phys.* **43**, 436 (1972).
- ⁵⁵J. R. Carruthers, E. G. Gibson, M. G. Klett, and B. R. Facemire, "Studies of rotating liquid floating zones on Skylab IV," *AIAA Paper No. 75-692*, 1975.
- ⁵⁶J. R. Carruthers, E. G. Gibson, M. G. Klett, and B. R. Facemire, "Studies of rotating liquid floating zones on Skylab IV," *Prog. Astronaut. Aeronaut.* **52**, 207 (1977).
- ⁵⁷R. Tagg, L. Cammack, A. Cronquist, and T. G. Wang, "Rotating liquid drops, Plateau's experiment revisited," Report No. JPL 900-954, Jet Propulsion Laboratory, Caltech, Pasadena, CA, 1980.
- ⁵⁸I. Martínez, "Liquid column stability," in *ESA SP-222* (ESA Publication Division, ESTEC, Noordwijk, 1984), p. 31.
- ⁵⁹I. Martínez, "Stability of long liquid columns in Spacelab-D1," in *ESA SP-256* (ESA Publication Division, ESTEC, Noordwijk, 1987), p. 235.
- ⁶⁰I. Martínez and J. Meseguer, "Floating liquid zones in microgravity," in

Scientific Results of the German Spacelab Mission D1 (DFVLR, Köln, 1987), p. 105.

- ⁶¹M. P. Elagin, A. P. Lebedev, and A. V. Tsmelev, "Laboratory modeling of the stability and dynamics of free liquid zones," in *Hydromechanics and Heat and Mass Transfer in Zero-Gravity* (Nauka, Moscow, 1982), p. 24 (in Russian).
- ⁶²I. Martínez, A. Sanz, J. M. Perales, and J. Meseguer, "Freezing of a liquid column on the Texus-18 Sounding Rocket Flight," *ESA J.* **12**, 483 (1988).
- ⁶³H. González, F. M. J. Mc Cluskey, A. Castellanos, and A. Barrero, "Stabilization of dielectric liquid bridges by electric fields in the absence of gravity," *J. Fluid Mech.* **206**, 545 (1989).
- ⁶⁴A. E. Green, "On the nonlinear behavior of fluid jets," *Int. J. Eng. Sci.* **14**, 49 (1976).
- ⁶⁵D. B. Bogoy, "Use of one-dimensional Cosserat theory to study instability in a viscous liquid jet," *Phys. Fluids* **21**, 190 (1978).
- ⁶⁶D. B. Bogoy, "Wave propagation and instability in a circular semi-finite liquid jet harmonically forced at the nozzle," *J. Appl. Mech.* **45**, 469 (1978).
- ⁶⁷D. B. Bogoy, "Breakup of a liquid jet, third perturbation Cosserat solution," *Phys. Fluids* **22**, 224 (1979).
- ⁶⁸D. B. Bogoy, "Drop formation in a circular liquid jet," *Annu. Rev. Fluid Mech.* **11**, 207 (1979).
- ⁶⁹A. Sanz-Andrés, J. M. Perales, P. Rodriguez de Francisco, and A. Sanz-Lobera, "A Plateau Tank Facility (PTF) for liquid bridge experimentation by using buoyancy technique for microgravity simulation," in *ESA SP-295* (ESA Publication Division, ESTEC, Noordwijk, 1990), p. 607.
- ⁷⁰C. Bisch, A. Lasek, and H. Rodot, "Comportement hydrodynamique de volumes liquides spheriques semi-libres en apesanteur simulée," *J. Méc. Théor. Appl.* **1**, 165 (1982).
- ⁷¹A. Sanz, "Comportamiento de las zonas líquidas flotantes en microgravedad simulada," Tesis doctoral, Universidad Politécnica de Madrid, 1983.
- ⁷²J. J. Stoker, *Nonlinear Vibrations* (Interscience, New York, 1966), Vol. II.

